รายงานวิจัยฉบับสมบูรณ์

โครงการ การพัฒนาโลหะออกไซด์และซัลไฟด์ที่มีโครงสร้างนาโนสำหรับเป็นตัวเร่งปฏิกิริยาดีออกซีจิเนชันในอนุพันธ์ชีวมวลเพื่อการผลิตเชื้อเพลิงชีวภาพ

โดย ดร.วรนุช อิทธิเบญจพงศ์

เดือน มิถุนายน ปี 2560

สัญญาเลขที่ TRG5880192

รายงานวิจัยฉบับสมบูรณ์

โครงการ การพัฒนาโลหะออกไซด์และซัลไฟด์ที่มีโครงสร้างนาโนสำหรับเป็นตัวเร่งปฏิกิริยาดีออกซีจิเนชันในอนุพันธ์ชีวมวลเพื่อการผลิตเชื้อเพลิงชีวภาพ

ผู้วิจัย ดร.วรนุช อิทธิเบญจพงศ์
สังกัด ศูนย์นาโนเทคโนโลยีแห่งชาติ
สำนักงานพัฒนาวิทยาศาสตร์และเทคโนโลยีแห่งชาติ

สนับสนุนโดยสำนักงานกองทุนสนับสนุนการวิจัยและศูนย์นาโนเทคโนโลยีแห่งชาติ สำนักงานพัฒนาวิทยาศาสตร์และเทคโนโลยีแห่งชาติ

Abstract (บทคัดย่อ)

Project Code : TRG5880192

(รหัสโครงการ) TRG5880192

Project Title : Development of nanostructured metal oxide and metal sulfide catalysts for deoxygenation of biomass derivatives to biofuels

(ชื่อโครงการ) การพัฒนาโลหะออกไซด์และซัลไฟด์ที่มีโครงสร้างนาโนสำหรับเป็นตัวเร่งปฏิกิริยาดีออกซีจิเนชันในอนุพันธ์ชีวมวลเพื่อการผลิตเชื้อเพลิงชีวภาพ

Investigator : Vorranutch Itthibenchapong, Ph.D. National Nanotechnology Center

(ชื่อนักวิจัย) ดร. วรนุช อิทธิเบญจพงศ์ ศูนย์นาโนเทคโนโลยีแห่งชาติ

E-mail Address : vorranutch@nanotec.or.th

Project Period : 2 years

(ระยะเวลาโครงการ) 2 ปี

Abstract The triglyceride-based feedstocks and biomass derivatives have been considered important resources for production of advanced biofuels, especially green renewable diesel and biojet fuels. Among the series of deoxygenation reactions, hydrodeoxygenation is a majority in the green diesel production when utilizing the group of metal sulfides catalysts, e.g. MoS_2 with various doping elements. Moreover, decarbonylation and decarboxylation are predominant over sulfur-free catalysts including noble metals, e.g., Pd and Pt, and non-precious transition metal, e.g., Ni. The research, development, and engineering of novel heterogeneous catalysts could be a key factor for commercialization and strong establishment of the biorefinery and biofuel industries.

บทคัดย่อ วัตถุดิบกลุ่มไทรกลีเซอร์ไรด์และอนุพันธ์ของชีวมวลถูกพิจารณาว่าเป็นทรัพยากรที่สำคัญสำหรับการผลิตเชื้อเพลิงชีวภาพขั้นสูงโดยเฉพาะอย่างยิ่งกลุ่มเชื้อเพลิงดีเซลหมุนเวียนและเชื้อเพลิงอากาศยานชีวภาพ ในกลุ่มปฏิกิริยาดีออกซิจิเนชัน ปฏิกิริยาไฮโดรดีออกซิจิเนชันเป็นปฏิกิริยาหลักในการผลิตเชื้อเพลิงดีเซลชีวภาพโดยใช้กลุ่มตัวเร่งปฏิกิริยาโลหะซัลไฟด์ เช่น โมลิบดินัมซัลไฟด์ (MoS_2) ร่วมกับธาตุชนิดอื่น นอกจากนี้ ในกลุ่มตัวเร่งปฏิกิริยาอื่นที่ปราศจากซัลเฟอร์ อาทิ โลหะหายากเช่น พัลลาเดียม (Pd) แพลทตินัม (Pt) และ โลหะทรานซิชัน เช่น นิกเคิล (Ni) จะมีความจำเพาะต่อกลุ่มปฏิกิริยาดีคาร์บอนิลเลชันและดีคาร์บอกซีเลชัน เป็นหลัก

ในงานวิจัย พัฒนา และวิศวกรรม ของตัวเร่งปฏิกิริยาวิวิธพันธุ์กลุ่มใหม่จะเป็นปัจจัยสำคัญในการนำไปใช้ประโยชน์เชิงพาณิชย์และสร้างรากฐานที่เข้มแข็งและมั่นคงของอุตสาหกรรมโรงกลั่นชีวภาพและเชื้อเพลิงชีวภาพ

Keywords : deoxygenation, biofuel, heterogeneous catalyst, diesel-like hydrocarbon, jet fuel-like hydrocarbon
(คำหลัก) ดีออกซิจิเนชัน, เชื้อเพลิงชีวภาพ, ตัวเร่งปฏิกิริยาวิวิธพันธุ์, ไฮโดรคาร์บอนที่มีองค์ประกอบคล้ายเชื้อเพลิงดีเซล, ไฮโดรคาร์บอนี่มีองค์ประกอบคล้ายเชื้อเพลิงอากาศยาน

Objectives

1. To develop the nanostructured catalysts based on transition metal sulfide and metal oxide on supporting materials by simple and low cost synthesis techniques.
2. To utilize the developed catalysts for the efficient production of the synthetic diesel and jet fuel-liked hydrocarbons.

In this project, the 3 catalyst systems will be discussed separately as listed below.

a) Deoxygenation of palm kernel oil to jet fuel-like hydrocarbons using Ni-MoS_2/γ-Al_2O_3 catalysts
b) Deoxygenation of oleic acid under an inert atmosphere using molybdenum oxide-based catalysts
c) Deoxygenation of Stearic acid into to diesel-range hydrocarbon using NiSn catalysts

Deoxygenation of palm kernel oil to jet fuel-like hydrocarbons using Ni-MoS_2/γ-Al_2O_3 catalysts

1. Introduction

Biofuels, such as biodiesel, bioethanol, biogas, and bio-oil, have played an important role as renewable energy for transportation and power generation due to the depletion of fossil fuel [1-5]. Deoxygenation, which removes oxygenated components from the reactants in the presence of hydrogen gas through hydrodeoxygenation (HDO) and decarbonylation (DCO) and without hydrogen consumption via decarboxylation (DCO2), has been used in various applications including bio-hydrogenated diesel (BHD) or green diesel production [6-8] and biomass upgrading into valuable chemicals [9]. The

HDO applied in the BHD technology has been proposed as a cleaner and more efficient pathway compared to DCO and DCO2 due to the lack of carbon loss from reactant conversion to hydrocarbons with the released of water as a by-product. However, DCO and DCO_2 lose one carbon atom to CO and CO_2 gas by-products, respectively, resulting in a liquid product with fewer carbons. The feedstock choices for renewable diesel production have been studied using various plant oils containing C16-C18 fatty acids as the main component including palm oil, rapeseed oil, jatropha oil, canola oil, and oil-extract from coffee ground [6, 8, 10-12]. Furthermore, waste-cooking oil, animal fat, and bio-oil have become potential feedstock candidates [13-16].

The deoxygenation catalysts employ various transition metals, metal sulfides, and metal phosphides on supports [9, 11, 17-24] (e.g., Al_2O_3, SiO_2, zeolite, and graphite). Co or Ni doped MoS_2 has been known as the state-of-the-art catalysts for HDO and hydrodesulfurization (HDS) because of their excellent catalytic performance and cost-effective application for large-scale production. The additional Ni in MoS_2 modifies the surface of MoS_2 to form a Ni-Mo-S phase which is known as the active site of $NiMoS_2$ catalyst [25]. The Ni or Co has proposed as a promoter to enhance catalytic activity of MoS_2 on a support [26, 27]. In addition, metal catalysts on oxide supports (e.g., Ni and Co on SiO_2 or Al_2O_3) are not only selective catalysts for DCO and DCO_2 over HDO [28-30], but also proposed to use for other applications such as Ni-based catalysts in methane reforming [31-33], de-NOx [34], and oxygen reduction reaction (ORR). [35, 36] The catalytic mechanism of Ni-MoS_2 has been studied computationally and experimentally in the unsupported catalyst systems [25, 37, 38]. The sulfur vacancies in MoS_2 have been proposed as the active sites for deoxygenation. The Ni atoms (dopants) favored the substitution into S-edges of MoS_2 structure, creating more sulfur vacancies and leading to enhancement of deoxygenation activity in Ni-MoS_2 with respect to MoS_2. In the system with a carboxylic acid reactant, the Ni promoter at the edge of the MoS_2 demonstrated the synergistic effect as the Ni-Mo-S phase which induced smaller activation energies in comparison to those of non-promoted MoS_2 for both the C=O hydrogenation and C-OH bond breaking steps [25]. The catalyst support in Ni-MoS_2 has been shown as the main source of catalyst acidity, i.e. Brønsted acid and/or Lewis acid, leading to isomerization and cracking reactions. The Al_2O_3 support is considered as a weakly-acidic support due to the majority of Al-octahedra in the structure compared with zeolites. Thus, Ni-MoS_2 on alumina support generally showed relatively low tendency of isomerization and cracking activities. Interestingly, the acidity modification of Al_2O_3 support (via Brønsted sites) has been reported as the positive

influence on the hydrogenation activity of the MoS_2 and Co-MoS_2 catalysts because of the direct change in their electronic properties [27].

Sulfidation by H_2S, CS_2, and dimethyldisulfide ($C_2H_6S_2$) are common in the synthesis of MoS_2-based catalysts. Nevertheless, the H_2S is a highly toxic gas that is expensive compared to other industrial gases, and therefore, special material-handling equipments are required. In addition, to allow the solid-gas phase reaction to produce a desirable phase, the formation of metal sulfide on the support may require a long preparation period. However, this long period may lead the aggregation of catalyst particles and ultimately a low surface area. Therefore, water-soluble sulfiding agents may promote sulfurization, which is applicable for preparation of supported catalysts and compatible with an impregnation method. Recently, thiourea ($CS(NH_2)_2$) was proposed for synthesis of unsupported MoS_2 catalysts [39-41]. However, MoS_2 on a support material prepared using this method has not been previously reported for the deoxygenation of biofuel. In our study, Ni-MoS_2 on a γ-Al_2O_3 support was prepared using thiourea sulfurization at low temperatures. The cooperation of Ni in the MoS_2 structure and interaction with Al_2O_3 were investigated using the X-ray absorption technique. The deoxygenation activities of the as-synthesized catalysts were studied using palm kernel oil, which is an abundant source of lauric acid (C12), to produce renewable jet fuel-like hydrocarbons. To provide a simple approach for large-scale preparation, sulfidation by thiourea in a liquid-phase processing will be compatible with a general synthesis method of unsupported and supported metal sulfide catalysts. The exploration of a new potential biojet fuel resource via triglyceride-feedstock conversion could provide a straightforward process for obtaining a high yield and tunable biojet fuel via deoxygenation and further isomerization.

2. Experimental

2.1 Catalyst preparation and characterization

The Ni-MoS_2/γ-Al_2O_3 catalyst was prepared by wetness impregnation with a precursor solution based on modification of our previously reported protocol [39] using thiourea as a sulfur agent. A mixture of nickel nitrate hexahydrate ($Ni(NO_3)_2{\cdot}6H_2O$, Sigma-Aldrich, 98.8%), $(NH_4)_6Mo_7O_{24}{\cdot}4H_2O$ (Carlo Erba, 99.0%), and thiourea ($CS(NH_2)_2$, Sigma-Aldrich, 99.0%) was dissolved in water with 1:20 molar ratio of molybdenum salt: thiourea. The solution containing a Ni /Ni+Mo ratio of 0.33 was stirred for 0.5-1 h prior to adding spherical γ-Al_2O_3 (1.8 mm of O.D., Sasol Company) at 85 wt.% of the catalyst followed by stirring at 60 °C for an additional 1-2 h. After

impregnation, the sample was dried in an oven for 10-12 h and calcined in an Ar atmosphere for 4 h at 400 °C with a heating rate of 10 °C min^{-1}. The final active phase Ni-MoS_2 was approximately 15 wt.% in the obtained catalyst. The actual molar ratio of Ni/(Ni+Mo) in the calcined catalyst was determined to be approximately 0.32 using inductively coupled plasma-optical emission spectrometry (ICP-OES). Phase identity of the catalyst was analyzed by X-ray diffraction (XRD) using a Bruker D8 Advance with Cu Kα radiation. The measurement was carried out at 40 kV and 40 mA and over a range of $10^o</2\theta<80^o$ (0.02 $deg.s^{-1}$ with a step time of 1 s. The Brunauer–Emmett–Teller (BET) surface area and Barrett-Joyner-Halenda (BJH) pore size of the catalysts were investigated by a N_2 sorption analyzer (Quanta Chrome NOVA2000e). The catalyst morphology was measured using transmission electron microscopy at 200 kV (TEM, TECNAI G2 20 S-Twin). The sample was ground into a fine powder and dispersed in methanol before mounted on a Cu grid coated with a thin film carbon for TEM analysis. The chemical state at the surface of the catalyst was analyzed by X-ray photoelectron spectroscopy (XPS, Kratos AXIS Ultra DLD). In our study, synchrotron-based X-ray absorption spectroscopy (XAS), which is a powerful structure-based technique, has been employed to study the electronic and local structural information of the materials [42]. The XAS spectra including X-ray absorption near edge structure (XANES) and extended X-ray absorption fine structure (EXAFS) spectra were acquired at the SUT-NANOTEC-SLRI XAS Beamline (BL 5.2) (bending magnet; electron energy of 1.2 GeV; beam current of 80–150 mA; 1.1 to 1.7x1011 photon s^{-1}) at the Synchrotron Light Research Institute (SLRI), Nakhon Ratchasima, Thailand. The Mo L3-edge and Ni K-edge spectra were collected in transmission mode using InSb(111) and Ge (220) double crystal monochromators with an energy resolution ($\Delta E/E$) of $2x10^{-4}$. The background correction and data fitting of the XANES and EXAFS data were done using the ATHENA and ARTEMIS programs in the IFEFFIT package [43, 44].

2.2 Catalytic reaction testing

Refined palm kernel oil and palm olein oil were commercially obtained from a local market in Thailand. As shown in **Table 1**, the fatty acid contents in the commercial oil were determined through fatty acid methyl esters (FAMEs) obtained by total transesterification of triglycerides at 65 ^oC for 4 h with methanol (9:1 mol ratio of methanol to oil) using a sodium methoxide ($NaOCH_3$) catalyst (1 wt% of oil). Acid value of the palm kernel oil was estimated by the titration method with KOH (0.1 M).

Table 1 Fatty acid content of commercial refined palm kernel oil compared to that of palm olein oil.

Fatty acid	Composition (wt.%)	
	palm olein oil	palm kernel oil
C8:0	-	1.2
C10:0	-	2.6
C12:0	0.4	48.8
C14:0	0.8	17.3
C16:0	37.4	-
C16:1	0.2	9.1
C18:0	3.6	2.1
C18:1	45.8	16.1
C18:2	11.1	2.3
C18:3	0.3	0.1
C20:0	0.3	-
C20:1	0.1	0.1

The palm olein oil consisted of C12–C20 fatty acids with oleic acid (C18:1) as the major component [45], which is preferred in synthetic diesel fuel production. The refined palm kernel oil (acid value of 0.26 mg KOH/g of oil) contained a high component of lauric acid (C12:0), which is suitable for biojet fuel application. The catalytic deoxygenation reactions were performed in a custom-made trickle-bed reactor with an internal diameter of 0.7 cm, length of 21 cm, and volume of 8.1 cm^3. After $NiMoS_2/Al_2O_3$ loading in the reactor, the system was pressurized with H_2 to the desired pressure and heated to the desired reaction temperature. The oil feeds were introduced to the reactor by a HPLC pump, and H_2 feed was controlled by mass flow controllers. The deoxygenation reactions were tested using the following conditions: reaction temperature of 270-330 °C, H_2 pressure of 30-50 bars, liquid hourly space velocity (LHSV) of 1-5 h^{-1}, and H_2/oil ratio of 1000 N(cm^3cm^{-3}). Each reaction parameter was evaluated using fresh catalyst to eliminate the effect of catalyst deactivation during the experiments. The three experiments using the same catalyst were performed and the liquid product was collected every 3 h interval for analysis. Thus, typically the total time

on stream on each reaction condition was 9 h while the catalytic activity remained stable.

Gas chromatograph instruments were used to identify the obtained products. A GC-2014 Shimadzu and a GC-MS Agilent 7890A equipped with DB-1HT (30 m x 0.32 mm x 0.1 μm) capillary columns were used for liquid product analysis. The calibration curve of standards was used to quantify a composition of n-alkanes in liquid products. In details, a diluted sample was injected into the GC with the split ratio of 100. An injection temperature of 340 ^{o}C, a detector temperature of 370 ^{o}C and a column temperature ramping from 40 to 270 ^{o}C) were used for the analysis. An online Shimadzu GC-14B equipped with molecular sieve 5A and Porapak Q packed columns was used for gas product analysis. The deoxygenation activities were calculated as shown in the following equations.

$$triglycerides\ conversion\ (\%) = \frac{mole\ of\ triglycerides\ in\ feed - mole\ of\ triglycerides\ in\ product\ (mole)}{mole\ of\ triglycerides\ in\ feed\ (mole)}\ x\ 100\% \quad \textbf{(1)}$$

$$Liquid\ product\ yield\ (\%) = \frac{totoal\ mole\ of\ n-alkanes\ in\ liquid\ product}{total\ mole\ of\ fatty\ acids\ in\ feed}\ x\ 100\% \quad \textbf{(2)}$$

$$HDO\ selectivity\ (\%) = \frac{total\ mole\ of\ n-alkanes\ (C8,C10,C12,C14,C16,C18)\ in\ liquid\ product}{total\ mole\ of\ fatty\ acids\ in\ feed}\ x\ 100\% \quad \textbf{(3)}$$

$$DCO + DCO2\ selectivity\ (\%) = \frac{total\ mole\ of\ n-alkanes\ (C7,C9,C11,C13,C15,C17)in\ liquid\ product}{total\ mole\ of\ fatty\ acids\ in\ feed}\ x\ 100\% \quad \textbf{(4)}$$

$$C10\ to\ C12\ selectivity\ (\%) = \frac{total\ mole\ of\ n-alkanes\ (C10,C11,C12)\ in\ liquid\ product}{total\ mole\ of\ fatty\ acids\ in\ feed}\ x\ 100\% \quad \textbf{(5)}$$

The heating values of the liquid products were also via a bomb calorimeter (LECO AC350), and the flow property was determined using automated cloud point and pour point analyzers (ISL CPP 5GS).

3. Results and Discussion

As shown in **Fig. 1**, the XRD pattern of a calcined Ni-MoS_2/γ-Al_2O_3 sample that was prepared using our new method with thiourea as a sulfiding agent indicated that the bulk phases of the catalysts on the γ-Al_2O_3 support included NiS_2 (PDF 03-065-3325), and MoS_2 corresponding to PDF 03-065-0160 as well as commercial MoS_2 (Sigma-Aldrich). The peak broadening shown in the XRD pattern of the catalyst was due to the semi-amorphous nature and small crystallite size (i.e., 5-10 nm determined by Scherrer's equation). Additionally, the broad MoS_2 peaks may indicate the low stacking and disorder of the MoS_2 layers. [46]

In addition, the Mo and Ni oxidation state and crystallinity of the bulk Ni-MoS_2/γ-Al_2O_3 material were confirmed by the XANES spectra [47] at Mo L_3-edges and Ni K-edges (**Fig. 2**). As shown in **Fig. 2(a)**, the Mo L_3-edge positions of Mo(0) (standard Mo metal foil, 2520.0 eV), Mo(IV) (MoS_2, 2522.3 eV) and Mo(VI) (MoO_3, α-$NiMoO_4$, 2524.1 eV) increased with the ionicity of the Mo bonding and electronegativity of the anions. The near-edge and post-edge features of the MoS_2-based compounds exhibited less intense amplitudes (low-k scattering), indicating poor crystallinity in the amorphous phase. Moreover, as seen in **Fig. 2(a)**, the white line intensity of Ni-MoS_2 became smaller and that of Ni-MoS_2/Al_2O_3 turned into higher when compared with that of MoS_2 standard, suggesting an existence of Ni-substitution in both samples. Besides, the Ni K-edge XANES spectra of Ni-MoS_2/ γ-Al_2O_3 compared to those of some Ni compounds indicated that the edge energy (at 8345.6 eV) was between those of the $NiAl_2O_4$ (8346.1eV), NiO (8345.9 eV), and NiS_2 (8339.4 eV) standards, as shown in **Fig. 2(b**). These results confirmed the presence of both Ni-S and Ni-O bonds, which may arise at the metal-support interface between Ni and MoS_2 and alumina, respectively. Based on the different post-edge features, unlike those in NiO and NiS_2 standards, this result also suggested the substitution of Ni into the MoS_2 and MoS_2/Al_2O_3 structures which is consistent with the observed Mo L3-edge XANES results. In order to clarify the Ni-substitution in samples, the EXAFS data at Ni K-edge is necessarily employed. The measured EXAFS spectra (black line) and the best fitting (red line) at Ni K-edge for the Ni-MoS_2 and Ni-MoS_2/Al_2O_3 samples are shown in **Fig. 3** (in real space), and the fitting parameters are listed in **Table 2**. The mean Ni-S and Ni-S/Ni-O coordination numbers and bonding distances around the Ni atoms in the MoS_2 and MoS_2/Al_2O_3 samples were 4.78(2) and 1.68(1)/3.40(2) and 2.223(4) Å and 2.204(1)/2.025(3) Å, respectively. These EXAFS results confirmed Ni substitution into the MoS_2 and MoS_2/Al_2O_3 structures, which is consistent with the reported XANES results. The metal doping in the based catalysts,

i.e. Ni or Co doping in MoS_2 [39, 48], Co doping in lattices of MoO_2[22], has been confirmed as the promoting effect to improve catalytic deoxygenation performance by modification of the electronic and geometric surface structure of the catalytic active sites via defects [48] e.g. S-vacancies in MoS_2.

However, the chemical state of the catalyst surface measured using the XPS technique (**Fig. 4a**) indicate the presence of at least two Mo species on the surface of the catalyst that exist as a mixture of Mo(IV) from MoS_2 and Mo(VI), which may arise from MoO_3 due to the formation of an oxide layer at the surface in contact with Al_2O_3. The peaks for Mo 3d5/2 at 229.0 eV and Mo3d3/2 at 232.1 eV were assigned to Mo(IV) in MoS_2, and the peaks for Mo3d3/2 at 232.9 eV and Mo 3d3/2 at 236.0 eV were assigned to Mo(VI) in MoO_3 [49, 50]. The presence of Ni (II) based on the XPS spectrum of Ni 2p was confirmed, as shown in **Fig. 4b.** The Ni 2p bands, the doublet 2p3/2 and 2p1/2 due to spin-orbit splitting, were fitted to the 3 species of Ni(II). The binding energy of Ni 2p3/2 around 854.6 eV could be related to the nickel sulfide compound (854-855 eV); this would be assigned for the NiS_2 in this case. The binding energy around 855.9 eV corresponded to Ni in $NiMoS_2/Al_2O_3$ [51] and the BE around 857.3 eV was close to either the Ni species in the interaction with the alumina support at the metal-support interface [52]. The broad bands around 860-865 eV and 878-885 eV were ascribable to the shake-up satellites structure of Ni(II) [51].

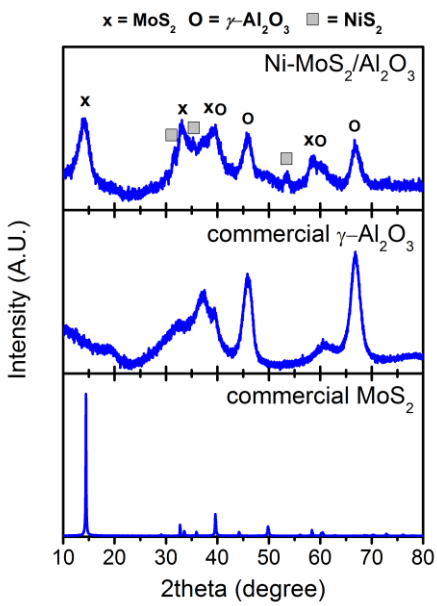

Fig. 1 XRD patterns of Ni-doped MoS_2/Al_2O_3 compared to those of commercial γ-Al_2O_3 and commercial MoS_2.

Table 2 Ni K-edge EXAFS fitting parameter of Ni-MoS_2/γ-Al_2O_3 prepared by thiourea sulfurization.

Samples	Paths	Coordination number (N)	σ^2	ΔE (eV)	R (Å)
Ni-MoS_2	Ni-S	4.78(2)	0.002	-6.916	2.223(4)
Ni-MoS_2/Al_2O_3	Ni-S	1.68(1)	0.005	-4.515	2.204(1)
	Ni-O	3.40(2)	0.007	-4.095	2.025(3)

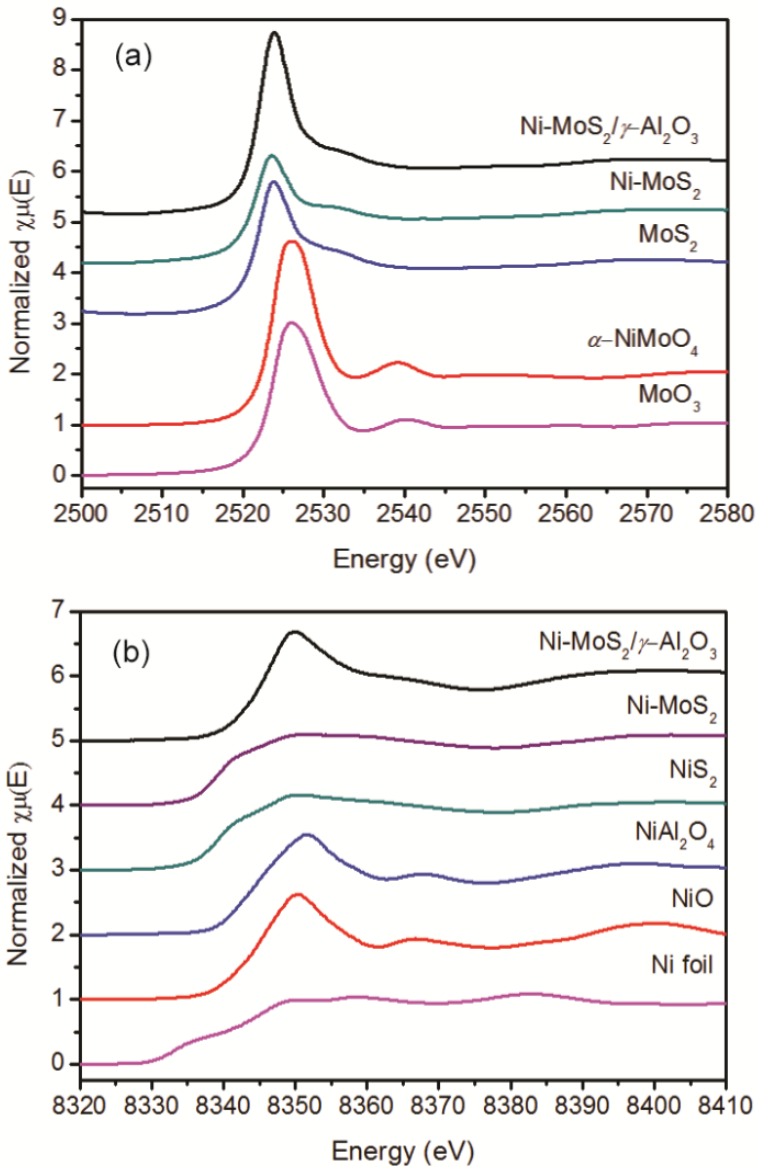

Fig. 2 (a) XANES spectra at Mo L_3-edges of Ni-MoS_2/γ-Al_2O_3 compared to those of Mo compounds and (b) XANES spectra at Ni K-edges of Ni-MoS_2/Al_2O_3 compared to those of Ni compounds.

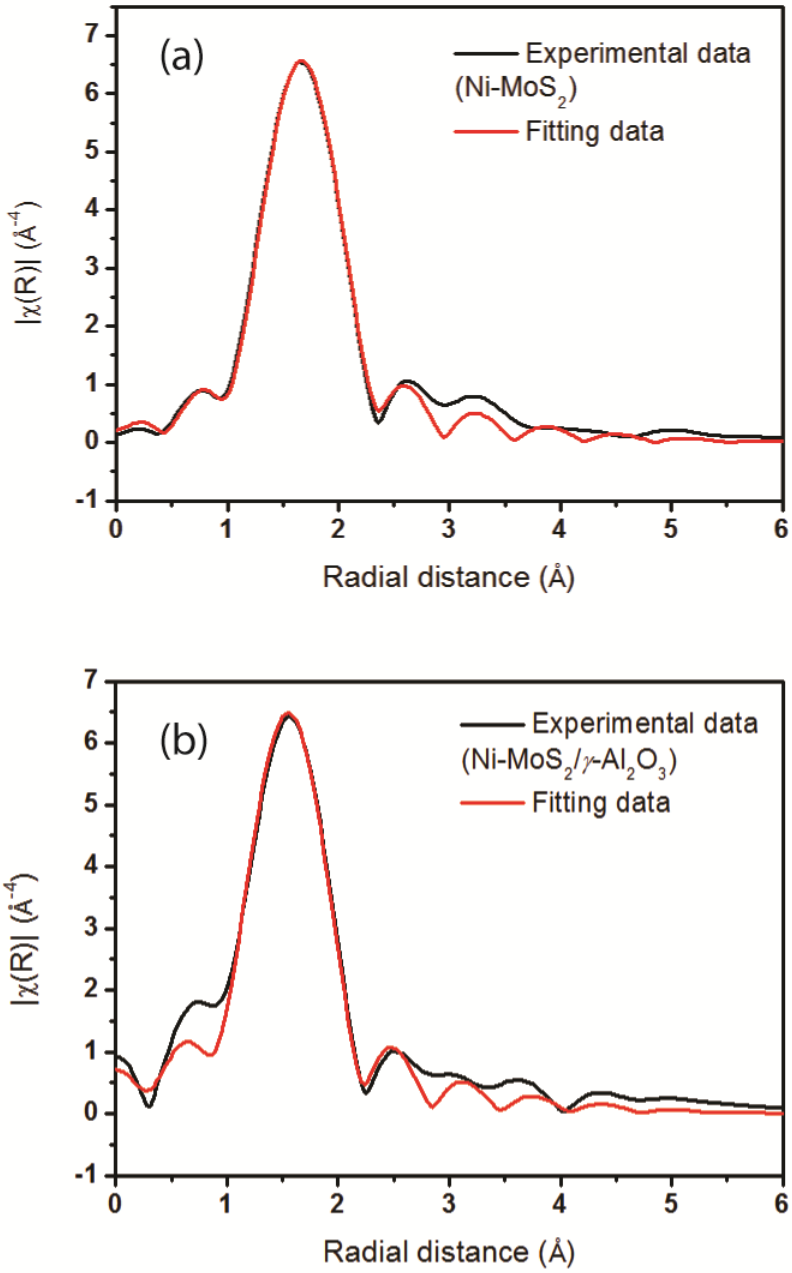

Fig. 3 Measured EXAFS data with the best fitting at the Ni K-edge for the Ni-MoS_2 and Ni-MoS_2/γ-Al_2O_3 samples.

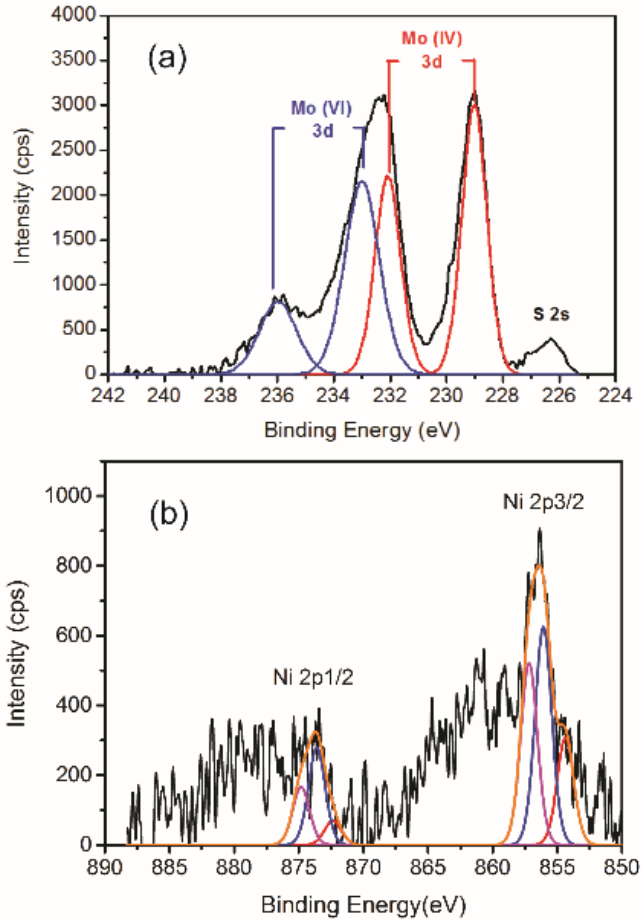

Fig. 4 XPS spectra of Ni-doped MoS_2/Al_2O_3: (a) Mo 3d and S 2s region and (b) Ni 2p region.

The layered structure of MoS_2 was observed in the TEM images (**Fig. 5**) as the dark line stacking, which represents a d(002) distance of 0.65 nm for crystalline MoS_2. This result is similar to the theoretical distance (0.62 nm), as shown in **Fig. 5(b)**. The number of layers was random and ranged from 1 to 4 layers (average of 1.8 layers), which is considered to be low stacking due to the low temperature synthesis [53]. The size of the MoS_2 sheets, which is the length of the dark lines, ranged from 2 to 9 nm (average of 4.1 nm), and the crystals of γ-Al_2O_3 support were approximately 5-20 nm in size. It should be noted that the particle size of the supported catalyst observed via an SEM technique was in a range of 0.5 to 5 □m, suggesting the agglomeration forms of the catalyst particles (results not shown). As shown in **Table 3**, the specific surface area of Ni-MoS_2/γ-Al_2O_3 synthesized using our method exhibited a slightly lower surface area, pore volume, and average pore size compared to that of γ-Al_2O_3 due to the deposition of Ni-MoS_2 on the surface and possibly inside the pores of the alumina.

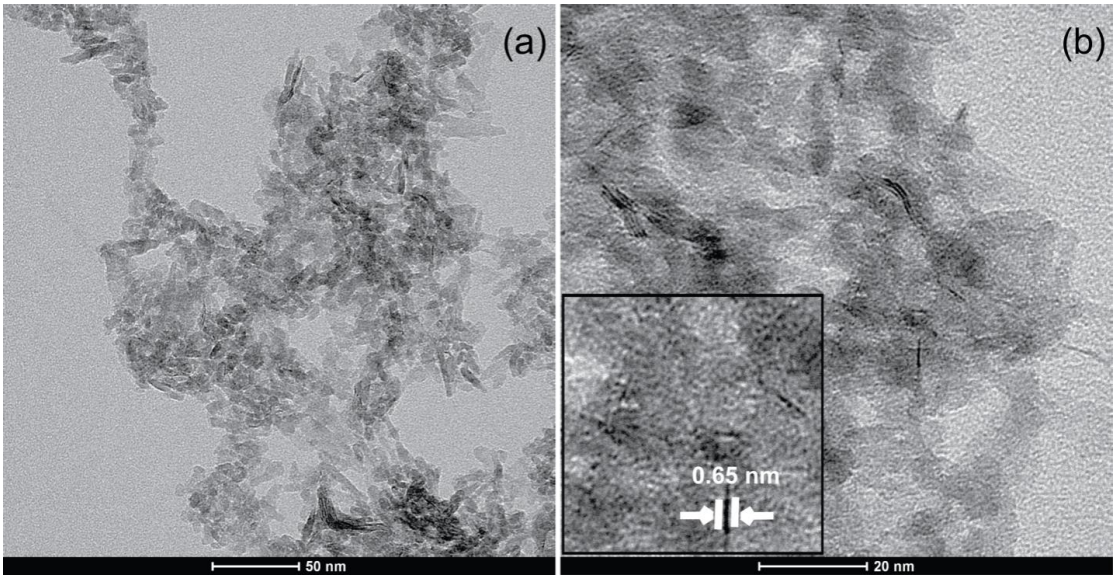

Fig. 5 TEM images of Ni-MoS_2/γ-Al_2O_3: (a) low magnification and (b) high magnification.

Table 3 Surface area and porous parameters of prepared catalysts.

Catalysts	S_{BET} ($m^2\ g^{-1}$)	Average BJH pore volume ($cm^3 g^{-1}$)	Average BJH pore diameter (nm)
γ-Al_2O_3	181	0.510	7.5
Ni-MoS_2/ γ-Al_2O_3	156	0.306	7.0

The deoxygenation of palm kernel oil using Ni-MoS_2/γ-Al_2O_3 under an excess H_2 atmosphere was performed with a custom-made trickle-based reactor. The proposed reaction pathways, represented in **Scheme 1,** were similar to those reported in different triglyceride feedstock [54, 55]. The triglycerides in palm kernel oil were degraded to propane gas and fatty acid molecules that consisted of primarily C12 with some C14 and C18, as shown in the **Table 1**. The deoxygenation of these fatty acids to obtain a biofuel product was proposed to occur via three main reactions. Hydrodeoxygenation (HDO), which is the primary H_2 consumption pathway, produced alkanes with the same number of carbon atoms as well as water as a by-product via C-O bond cleavage. Decarbonylation (DCO), which used the least H_2, and decarboxylation (DCO_2), which does not use H_2, produced alkanes via C-C bond cleavage leading to the loss of one carbon atom to CO gas and water (DCO) and CO_2 gas (DCO_2), respectively.

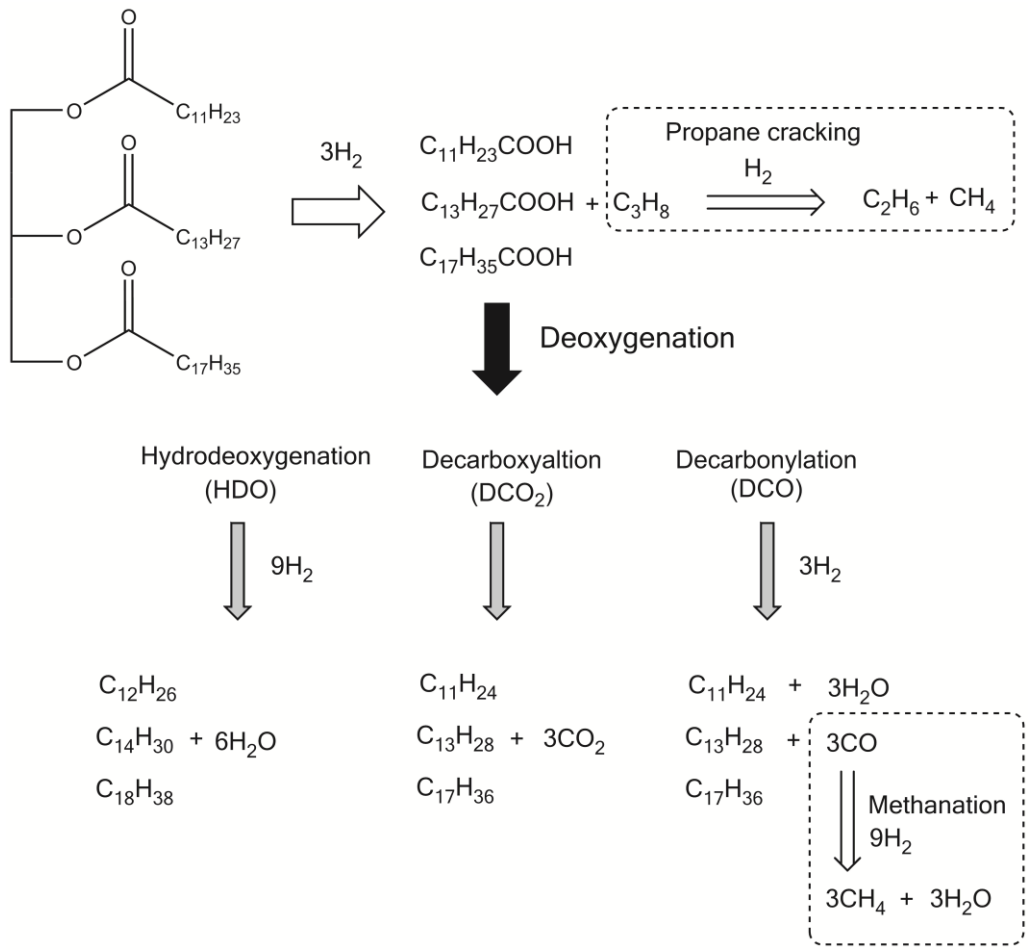

Scheme 1 Proposed catalytic palm kernel oil conversion via deoxygenation into jet diesel-like hydrocarbons.

As shown in **Fig. 6a**, an increase in the reaction temperature under a H_2 pressure of 50 bar and LHSV of 1 h^{-1} enhanced the yield due to improvement in the product yield via DCO_2 and DCO reactions. However, the selectivity to the HDO product was slightly higher when comparing those at 270 °C and 300 °C and slightly lower at 330 °C, and the selectivity of the competitive DCO_2 + DCO reactions increased based on gas product distribution (**Fig. 6b**). These results are in good agreement with the exothermic nature of HDO [56], which is unfavorable at higher temperature. Nevertheless, the HDO pathway still dominated the total reactions at 270-330 °C. Cracking as a side reaction tended to occur at high temperatures, especially propane cracking at 330 °C based on an increase in the ethane composition in the gas product. Moreover, methanation (i.e., CO conversion to CH_4) may occur starting at 300 °C due to a decrease in CO, which was inversely proportional to CO_2 accumulation. It should be noted that the C10-C12 selectivity in the liquid product remained almost constant at all reaction temperatures. In the study of the LHSV parameter, a shorter contact time

between the reactant and the catalyst (high LHSV) led to a significant decrease in the HDO product contribution and a small increase in the DCO_2+DCO product contribution, which resulted in a decrease in the total yield (**Fig. 7a**). Moreover, the CO distribution in the gas product increased at a high LHSV, indicating that the DCO pathway is favored at a short resident time (**Fig. 7b**). As the H_2 pressure increased (**Fig. 8a**), the liquid yield increased as a result of the domination of the HDO activity under the H_2 rich conditions at the catalyst surface over those from the DCO_2 + DCO pathways due to the large H_2 consumption required in the HDO pathway [10, 54]. The CO amount in the gas product was suppressed at H_2 pressure of 50 bar, and the CO_2 level remained similar to that at lower H_2 pressures (**Fig. 8b**). It is important to note that methanation, which is favorable under high H_2 pressure conditions [57], may have occurred at a H_2 pressure of 50 bar based on the slight increase in the methane amount compared to that of ethane. The turnover frequency (TOF), the generation rate of liquid product per the active site determined by CO uptake, was 0.0260 s^{-1} for the condition of 330 ^{o}C, H_2 pressure of 5 MPa, and LHSV of 1 h^{-1}.

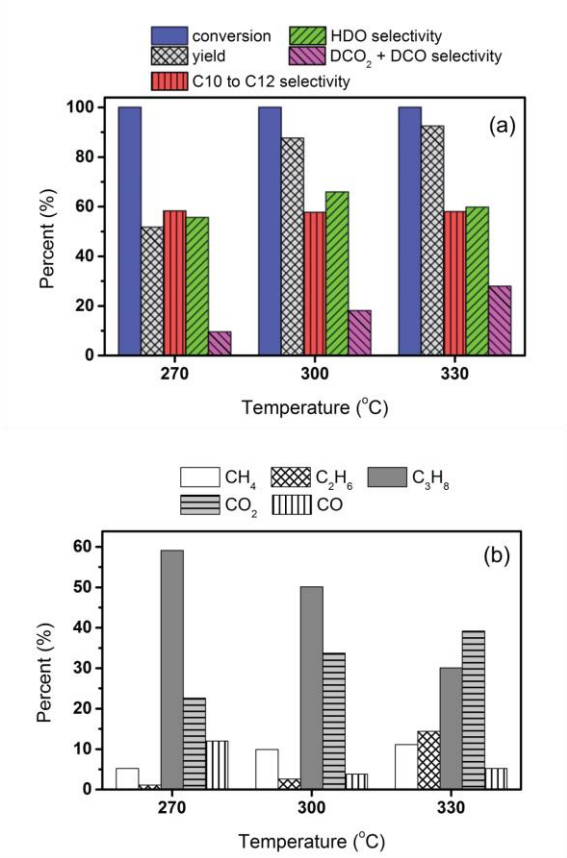

Fig. 6 Effect of reaction temperature on deoxygenation of palm kernel oil under a H_2 pressure of 50 bar and LHSV of 1 h^{-1}: (a) catalytic performance based on liquid product and (b) gas product distribution (%mol).

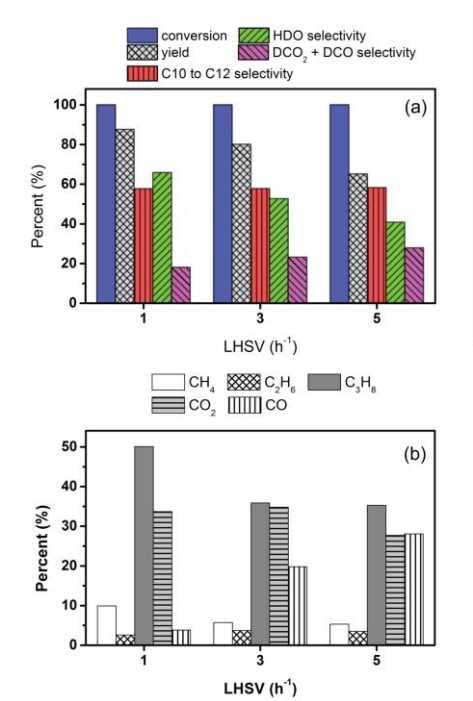

Fig. 7 Effect of LHSV on deoxygenation of palm kernel oil at 300 °C and a H_2 pressure of 50 bar: (a) catalytic performance based on liquid product and (b) gas product distribution (%mol).

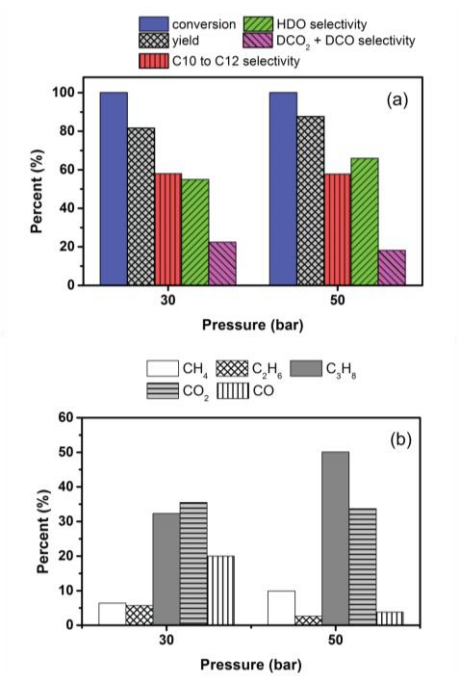

Fig. 8 Effect of H_2 pressure on deoxygenation of palm kernel oil at 300 °C and a LHSV of 1 h^{-1}: (a) catalytic performance based on liquid product and (b) gas product distribution (%mol).

The conversion of palm kernel oil was >99% under various operational conditions in the current study (i.e., reaction temperature, LHSV, and H_2 pressure). Therefore, the selectivity to C10-C12 alkanes in the liquid product remained at approximately 58%, corresponding to the amount of lauric acid in the palm kernel oil feedstock. In addition, the catalytic activities of the different oil feedstocks (i.e., palm kernel oil and palm olein oil) based on the yield contributed by the high HDO product selectivity were similar (result not shown). Therefore, the fatty acid chain did not significantly affect the deoxygenation performance over the Ni-MoS_2/γ-Al_2O_3 catalyst under the studied conditions. Depending on the product composition, the liquid biofuel from palm kernel oil consisted of jet fuel-like hydrocarbons, and product from palm olein oil consisted of diesel-like hydrocarbons. The differences in heating value and cold flow property of biofuel products from the two feedstocks were in association with the composition of the alkanes based on their fatty acid origins. The medium chain alkanes (i.e., C10-C12) in the product obtained from palm kernel oil improved the cloud point (6.2 ^{o}C) and pour point (-3.0 ^{o}C) while maintaining an excellent high heating value of 46.6 MJ kg^{-1} comparable to the green diesel from palm olein. Typically, the commercial jet fuels contain additives to keep low freezing point, cloud point and pour point, leading to excellent cold flow properties at actual working conditions. The fuel property and chemical composition of the additive-free jet fuel-like hydrocarbons in this work could be suitable for blending with fossil jet or diesel range fuel.

4. Conclusions

A novel method for metal sulfide preparation using thiourea sulfurization under an inert atmosphere was successfully applied for the synthesis of the Ni-MoS_2/γ-Al_2O_3 catalyst. The catalytic performance for the deoxygenation of palm kernel oil was studied as an alternative approach for the production of jet fuel-like hydrocarbons. A high HDO activity, which was the major pathway for deoxygenation, was observed a high H_2 pressure was applied at 300 °C with a long contact time (low LHSV) between the reactants and the catalyst. The promotion of DCO_2 and DCO occurred as the reaction temperature increased and with a short resident time (fast LHSV). The side reactions, such as cracking and methanation, occurred at high temperatures, such as 330 °C. The optimum product yield was approximately 92%, which was primarily from the HDO product (~60%) with 58% selectivity to C10-C12 for the jet fuel-like hydrocarbons under

the following conditions: 330 °C, H_2 pressure of 50 bar, LHSV of 1 h^{-1}, and H_2/oil ratio of 1000 N(cm^3 cm^{-3}).

References

[1] DemirbaŞ A. Biomass resource facilities and biomass conversion processing for fuels and chemicals. Energy Convers Manage 2001;42:1357-78.

[2] Chheda JN, Huber GW, Dumesic JA. Liquid-phase catalytic processing of biomass-derived oxygenated hydrocarbons to fuels and chemicals. Angew Chem Int Ed Engl 2007;46:7164-83.

[3] R. dos Santos T, Harnisch F, Nilges P, Schröder U. Electrochemistry for biofuel generation: Transformation of fatty acids and triglycerides to diesel-like olefin/ether mixtures and olefins. ChemSusChem 2015;8:886-93.

[4] Mansir N, Taufiq-Yap YH, Rashid U, Lokman IM. Investigation of heterogeneous solid acid catalyst performance on low grade feedstocks for biodiesel production: A review. Energy Convers Manage 2016;In Press.

[5] Soltani S, Rashid U, Al-Resayes SI, Nehdi IA. Recent progress in synthesis and surface functionalization of mesoporous acidic heterogeneous catalysts for esterification of free fatty acid feedstocks: A review. Energy Convers Manage 2016;In Press.

[6] Srifa A, Faungnawakij K, Itthibenchapong V, Viriya-Empikul N, Charinpanitkul T, Assabumrungrat S. Production of bio-hydrogenated diesel by catalytic hydrotreating of palm oil over NiMoS2/□-Al2O3 catalyst. Bioresour Technol 2014;158:81-90.

[7] Han J, Duan J, Chen P, Lou H, Zheng X, Hong H. Carbon-supported molybdenum carbide catalysts for the conversion of vegetable oils. ChemSusChem 2012;5:727-33.

[8] Phimsen S, Kiatkittipong W, Yamada H, Tagawa T, Kiatkittipong K, Laosiripojana N, et al. Oil extracted from spent coffee grounds for bio-hydrotreated diesel production. Energy Convers Manage 2016;126:1028-36.

[9] Alonso DM, Wettstein SG, Dumesic JA. Bimetallic catalysts for upgrading of biomass to fuels and chemicals. Chem Soc Rev 2012;41:8075-98.

[10] Liu Y, Sotelo-Boyás R, Murata K, Minowa T, Sakanishi K. Hydrotreatment of vegetable oils to produce bio-hydrogenated diesel and liquefied petroleum gas fuel over catalysts containing sulfided Ni–Mo and solid acids. Energy Fuels 2011;25:4675-85.

[11] Wang C, Tian Z, Wang L, Xu R, Liu Q, Qu W, et al. One-step hydrotreatment of vegetable oil to produce high quality diesel-range alkanes. ChemSusChem 2012;5:1974-83.

[12] Kubička D, Horáček J. Deactivation of HDS catalysts in deoxygenation of vegetable oils. Appl Catal, A 2011;394:9-17.

[13] Toba M, Abe Y, Kuramochi H, Osako M, Mochizuki T, Yoshimura Y. Hydrodeoxygenation of waste vegetable oil over sulfide catalysts. Catal Today 2011;164:533-7.

[14] Bezergianni S, Kalogianni A, Dimitriadis A. Catalyst evaluation for waste cooking oil hydroprocessing. Fuel 2012;93:638-41.

[15] Kaewmeesri R, Srifa A, Itthibenchapong V, Faungnawakij K. Deoxygenation of waste chicken fats to green diesel over Ni/Al2O3: Effect of water and free fatty acid content. Energy Fuels 2015:150116163647003.

[16] Puértolas B, Keller TC, Mitchell S, Pérez-Ramírez J. Deoxygenation of bio-oil over solid base catalysts: From model to realistic feeds. Appl Catal, B 2016;184:77-86.

[17] Popov A, Kondratieva E, Goupil JM, Mariey L, Bazin P, Gilson J-P, et al. Bio-oils hydrodeoxygenation: Adsorption of phenolic molecules on oxidic catalyst supports. J Phys Chem C 2010;114:15661-70.

[18] Wu S-K, Lai P-C, Lin Y-C, Wan H-P, Lee H-T, Chang Y-H. Atmospheric hydrodeoxygenation of guaiacol over alumina-, zirconia-, and silica-supported nickel phosphide catalysts. ACS Sus Chem Eng 2013;1:349-58.

[19] Teerawit Prasomsri TN, Yuriy Román-Leshkov. Effective hydrodeoxygenation of biomass-derived oxygenates into unsaturated hydrocarbons by MoO3 using low H2 pressures. Energy Environ Sci 2013;6:1732-8.

[20] Chen L, Fu J, Yang L, Chen Z, Yuan Z, Lv P. Catalytic hydrotreatment of fatty acid methyl esters to diesel-like alkanes over Hβ zeolite-supported nickel catalysts. ChemCatChem 2014;6:3482-92.

[21] Yeh T, Linic S, Savage PE. Deactivation of Pt catalysts during hydrothermal decarboxylation of butyric acid. ACS Sus Chem Eng 2014;2:2399-406.

[22] Ding R, Wu Y, Chen Y, Chen H, Wang J, Shi Y, et al. Catalytic hydrodeoxygenation of palmitic acid over a bifunctional Co-doped MoO2/CNTs catalyst: an insight into the promoting effect of cobalt. Catal Sci Tech 2016.

[23] Silva LN, Fortes ICP, de Sousa FP, Pasa VMD. Biokerosene and green diesel from macauba oils via catalytic deoxygenation over Pd/C. Fuel 2016;164:329-38.

[24] Al-Muhtaseb AaH, Jamil F, Al-Haj L, Al-Hinai MA, Baawain M, Myint MTZ, et al. Efficient utilization of waste date pits for the synthesis of green diesel and jet fuel fractions. Energy Convers Manage 2016;127:226-32.

[25] Ruinart de Brimont M, Dupont C, Daudin A, Geantet C, Raybaud P. Deoxygenation mechanisms on Ni-promoted MoS2 bulk catalysts: A combined experimental and theoretical study. J Catal 2012;286:153-64.

[26] Okamoto Y, Hioka K, Arakawa K, Fujikawa T, Ebihara T, Kubota T. Effect of sulfidation atmosphere on the hydrodesulfurization activity of SiO2-supported Co–Mo sulfide catalysts: Local structure and intrinsic activity of the active sites. J Catal 2009;268:49-59.

[27] Chen W, Maugé F, van Gestel J, Nie H, Li D, Long X. Effect of modification of the alumina acidity on the properties of supported Mo and CoMo sulfide catalysts. J Catal 2013;304:47-62.

[28] Kim SK, Brand S, Lee H-s, Kim Y, Kim J. Production of renewable diesel by hydrotreatment of soybean oil: Effect of reaction parameters. Chem Eng J 2013;228:114-23.

[29] Srifa A, Viriya-empikul N, Assabumrungrat S, Faungnawakij K. Catalytic behaviors of Ni/□-Al2O3 and Co/□-Al2O3 during the hydrodeoxygenation of palm oil. Catal Sci Tech 2015;5:3693-705.

[30] Li G, Zhang F, Chen L, Zhang C, Huang H, Li X. Highly selective hydrodecarbonylation of oleic acid into n-heptadecane over a supported nickel/zinc oxide–alumina catalyst. ChemCatChem 2015;7:2646-53.

[31] Zhao X, Li H, Zhang J, Shi L, Zhang D. Design and synthesis of NiCe@m-SiO2 yolk-shell framework catalysts with improved coke- and sintering-resistance in dry reforming of methane. Int J Hydrogen Energy 2016;41:2447-56.

[32] Xie T, Shi L, Zhang J, Zhang D. Immobilizing Ni nanoparticles to mesoporous silica with size and location control via a polyol-assisted route for coking- and sintering-resistant dry reforming of methane. Chem Commun (Camb) 2014;50:7250-3.

[33] Cao Y, Li H, Zhang J, Shi L, Zhang D. Promotional effects of rare earth elements (Sc, Y, Ce, and Pr) on NiMgAl catalysts for dry reforming of methane. RSC Adv 2016;6:112215-25.

[34] Cai S, Zhang D, Shi L, Xu J, Zhang L, Huang L, et al. Porous Ni-Mn oxide nanosheets in situ formed on nickel foam as 3D hierarchical monolith de-NOx catalysts. Nanoscale 2014;6:7346-53.

[35] Kariuki NN, Cansizoglu MF, Begum M, Yurukcu M, Yurtsever FM, Karabacak T, et al. SAD–GLAD Pt–Ni@Ni nanorods as highly active oxygen reduction reaction electrocatalysts. ACS Catal 2016;6:3478-85.

[36] Li B, Zhang L, Chen L, Cai X, Lai L, Wang Z, et al. Graphene-supported non-precious metal electrocatalysts for oxygen reduction reactions: the active center and catalytic mechanism. J Mater Chem A 2016;4:7148-54.

[37] Kibsgaard J, Tuxen A, Knudsen KG, Brorson M, Topsøe H, Lægsgaard E, et al. Comparative atomic-scale analysis of promotional effects by late 3d-transition metals in MoS2 hydrotreating catalysts. J Catal 2010;272:195-203.

[38] Zhang H, Lin H, Zheng Y. The role of cobalt and nickel in deoxygenation of vegetable oils. Appl Catal, B 2014;160–161:415-22.

[39] Itthibenchapong V, Ratanatawanate C, Oura M, Faungnawakij K. A facile and low-cost synthesis of MoS2 for hydrodeoxygenation of phenol. Catalysis Communications 2015;68:31-5.

[40] Wang W, Li L, Wu K, Zhu G, Tan S, Li W, et al. Hydrothermal synthesis of bimodal mesoporous MoS2 nanosheets and their hydrodeoxygenation properties. RSC Adv 2015;5:61799-807.

[41] Liu N, Guo Y, Yang X, Lin H, Yang L, Shi Z, et al. Microwave-assisted reactant-protecting strategy toward efficient MoS2 electrocatalysts in hydrogen evolution reaction. ACS Appl Mater Interfaces 2015;7:23741-9.

[42] Rehr JJ, Albers RC. Theoretical approaches to x-ray absorption fine structure. Rev Mod Phys 2000;72:621-54.

[43] Newville M. EXAFS analysis using FEFF and FEFFIT. J Synchrotron Radiat 2001;8:96-100.

[44] Ravel B, Newville M. ATHENA, ARTEMIS, HEPHAESTUS: data analysis for X-ray absorption spectroscopy using IFEFFIT. J Synchrotron Radiat 2005;12:537-41.

[45] Viriya-Empikul N, Krasae P, Puttasawat B, Yoosuk B, Chollacoop N, Faungnawakij K. Waste shells of mollusk and egg as biodiesel production catalysts. Bioresour Technol 2010;101:3765-7.

[46] Chianelli RRP, E. B.; Pecoraro, T. A.; Deneufville, J. P. Molybdenum disulfide in the poorly crystalline "Rag" structure. Science 1979;203:1105-7.

[47] Surisetty VR, Hu Y, Dalai AK, Kozinski J. Structural characterization and catalytic performance of alkali (K) and metal (Co and Rh)-promoted MoS2 catalysts for higher alcohols synthesis. Appl Catal, A 2011;392:166-72.

[48] Jeppe V. Lauritsena JK, Georg H. Olesena, Poul G. Moses, Berit Hinnemann, Stig Helveg, Jens K. Nørskov, Bjerne S. Clausen, Henrik Topsøe, Erik Lægsgaard, Flemming Besenbacher Location and coordination of promoter atoms in Co- and Ni-promoted MoS2-based hydrotreating catalysts. J Catal 2007;249:220-33.

[49] Katrib A, Benadda A, Sobczak JW, Maire G. XPS and catalytic properties of the bifunctional supported MoO2(Hx)ac on TiO2 for the hydroisomerization reactions of hexanes and 1-hexene. Appl Catal, A 2003;242:31-40.

[50] Baker MA, Gilmore R, Lenardi C, Gissler W. XPS investigation of preferential sputtering of S from MoS2 and determination of MoSx stoichiometry from Mo and S peak positions. Appl Surf Sci 1999;150:255-62.

[51] Mérida-Robles J, Rodrı guez-Castellón E, Jiménez-López A. Characterization of Ni, Mo and Ni–Mo catalysts supported on alumina-pillared α-zirconium phosphate and reactivity for the thiophene HDS reaction. J Mol Catal A: Chem 1999;145:169-81.

[52] Guichard B, Roy-Auberger M, Devers E, Legens C, Raybaud P. Aging of Co(Ni)MoP/Al2O3 catalysts in working state. Catal Today 2008;130:97-108.

[53] Kumar KS, Li W, Choi M, Kim SM, Kim J. Synthesis and lithium storage properties of MoS2 nanoparticles prepared using supercritical ethanol. Chem Eng J 2016;285:517-27.

[54] KubiČka D, Kaluža L. Deoxygenation of vegetable oils over sulfided Ni, Mo and NiMo catalysts. Appl Catal, A 2010;372:199-208.

[55] Kim SK, Han JY, Lee H-s, Yum T, Kim Y, Kim J. Production of renewable diesel via catalytic deoxygenation of natural triglycerides: Comprehensive understanding of reaction intermediates and hydrocarbons. Appl Energy 2014;116:199-205.

[56] Snåre M, KubiČková I, Mäki-Arvela P, Eränen K, Murzin DY. Heterogeneous catalytic deoxygenation of stearic acid for production of biodiesel. Ind Eng Chem Res 2006;45:5708-15.

[57] Gao J, Wang Y, Ping Y, Hu D, Xu G, Gu F, et al. A thermodynamic analysis of methanation reactions of carbon oxides for the production of synthetic natural gas. RSC Adv 2012;2:2358-68.

[58] Zabarnick S, Widmor N. Studies of jet fuel freezing by differential scanning calorimetry. Energy Fuels 2001;15:1447-53.

[59] Chuck CJ, Donnelly J. The compatibility of potential bioderived fuels with Jet A-1 aviation kerosene. Appl Energy 2014;118:83-91.

[60] Bezergianni S, Dimitriadis A, Kalogianni A, Knudsen KG. Toward hydrotreating of waste cooking oil for biodiesel production. effect of pressure, H2/Oil ratio, and liquid hourly space velocity. Ind Eng Chem Res 2011;50:3874-9.

[61] Guzman A, Torres JE, Prada LP, Nuñez ML. Hydroprocessing of crude palm oil at pilot plant scale. Catal Today 2010;156:38-43.

Deoxygenation of oleic acid under an inert atmosphere using molybdenum oxide-based catalysts

1. Experimental

1.1 Catalyst preparation

Bimetal NiMo oxide catalysts were prepared by impregnating a commercial γ-Al_2O_3 (Sasol company, Germany) with $(NH_4)_6Mo_7O_{24}\cdot 4H_2O$ (Carlo Erba) and $Ni(NO_3)_2\cdot 6H_2O$ (Ajax Finechem) solution containing 0.3 atomic ratio of Ni/(Ni + Mo). Next, the samples were dried at 65°C for 12 h and then calcined at 500°C for 5 h in air. The catalysts with metal loading on alumina (wt.%) of 19%, 27%, and 34% were denoted as 19NiMo-Al, 27NiMo-Al, and 34NiMo-Al, respectively. Furthermore, the 19NiMo-Al was reduced at 500°C for 3 h in H_2 flow and collected in N_2 atmosphere, which denoted as 19NiMo-Al (Red.) to compare active phase and catalytic activity with the non-reduced catalysts. Also, the monometal Mo oxide and other bimetal CuMo and CoMo oxides on alumina were prepared similarly to that of 19NiMo-Al and denoted as 19Mo-Al, 19CuMo-Al, and 19CoMo-Al, respectively using $Cu(NO_3)_2\cdot 4H_2O$ (Carlo Erba) and $Co(NO_3)_2\cdot 6H_2O$ (Carlo Erba) as Cu and Co precursors.

1.2 Catalyst characterization

The phase identity of as-synthesized catalysts was investigated via a Bruker D8 Advance X-ray diffraction (XRD) using Cu Kα source at 40 kV and 40 mA and collecting 2theta scan ranges from 10° to 80° with a step of $0.02°s^{-1}$. Surface area and porosity were determined by N_2-adsorption-desorption technique at -196 ^oC on a Quantachrome Instruments Nova 2000e surface area analyzer. The specific surface area was estimated by the Brunauer-Emmett-Teller (BET) equation and pore size and pore diameter were calculated by the Barrett–Joyner–Hallenda (BJH) method. Morphology, elemental distribution, and crystallization of the catalysts were examined by field emission scanning electron microscope/energy dispersive X-ray spectroscopy (FE-SEM/EDX, Hitachi SU8030) and transmission electron microscopy (TEM, JEOL 2100). The reducibility of as-synthesized catalyst was investigated by temperature-programmed reduction (TPR) using a Quantachrome ChemBET pulsar TPR/TPD instrument. The sample was pretreated at 120°C for 3 h under Helium atmosphere prior to the measurement. The reduction was carried out from 40 to 950 °C under 5 vol.% H_2 in argon gas with a similar flow rate at 30 mL/min. The surface species of as-synthesized catalyst was determined by X-ray photoelectron spectroscopy (XPS) using a PHI 5000

Versa Probe II XPS system (ULVAC-PHI, Japan). Binding energies were calibrated by C 1s species at 284.9 eV.

1.3 Catalytic deoxygenation testing and product analysis

Deoxygenation reactions were carried out in a 300 mL of Parr 4568 batch reactor. An oleic acid (Aldrich, technical grade, 90% purity) was used as a model compound of palm oil without further purification with catalyst loading of 20% w/w of reactant, i.e. 6 g of catalyst and 30 g of oleic acid. The reaction testing was performed under these conditions: N_2 pressurizing at room temperature (10 to 40 bar), stirring rate of 450 rpm, reaction temperature of 300 to 350 ^{o}C, and reaction time of 3 to 9 h. Liquid products, which mainly consisted of n-paraffin, stearic acid, and oleic acid, were analyzed by a GC-MS (Agilent Technologies, 7890A) and a GC-FID (GC-2014, Shimadzu) equipped with DB-1HT columns (30m x 0.32mm x 0.1μm). The gas products were analyzed by a GC-TCD (Shimadzu GC-14B) equipped with molecular sieve 5A and Porapak Q columns. The oleic acid conversion and liquid product distribution were calculated by using the following equations:

$$\%conversion = \frac{oleic\ acid\ in\ feed\ (g) - oleic\ acid\ in\ products\ (g)}{oleic\ acid\ in\ feed\ (g)} \times 100\% \quad \mathbf{Eq.(1)}$$

$$\%\ product\ A\ distribution\ = \frac{weight\ of\ product\ A}{weight\ of\ total\ liquid\ products} \times 100\% \quad \mathbf{Eq.(2)}$$

2. Results and discussion

2.1 Catalyst characterization

Illustrated in **Fig. 1**, the XRD patterns of as-synthesized catalysts revealed apparently broaden peaks of γ-alumina (ICDD PDF 00-001-1303) as the catalyst support with an average crystallite size of 5.4 nm determined by the Scherrer equation, while the small peaks indicated mixed phases of metal oxides. In **Fig. 1a**, the 19Mo-Al peak patterns demonstrated crystalline α-MoO_3 phase (ICDD PDF 01-074-7383). The various Ni-doping concentrations in NiMo-Al catalysts (**Fig. 1b, 1c, and 1d)** yielded the mixed phases of α-MoO_3 and α-$NiMoO_4$ (ICDD PDF 00-033-0948) with the enhancement of peak intensities corresponding to the increase of %metal oxides loading in catalysts. Moreover, XRD patterns of the samples with the Co and Cu doping in Mo-Al (**Fig. 1e and 1f)** showed the formation of $CoMoO_4$ (ICDD PDF 00-021-0868) and $CuMoO_4$ (ICDD PDF 01-077-0699) phases, respectively, along with α-MoO_3 phase

similarly to those in NiMo-Al catalysts. In case of the 19NiMo-Al (Red.) catalyst, which was reduced under the H_2 gas (**Fig.1g**), the α-MoO_3 and α-$NiMoO_4$ were transformed to MoO_2 (ICDD PDF 01-074-4517) and Ni metal (ICDD PDF00-004-0850) indicating the reduction of Mo^{6+} to Mo^{4+} and Ni^{2+} to Ni^0 which would act as active sites in a typical hydrodeoxygenation reaction under H_2 atmosphere. [27] In addition, confirmed by the H_2-TPR profile of 19NiMo-Al catalyst (**Fig. 2),** the four principle peaks for H_2 consumption corresponded to the reduction processes of Mo^{6+} to Mo^{4+} (around 520°C), Ni^{2+} to Ni^0 with strong interaction with molybdenum oxide (620 to 700 °C), and Mo^{4+} to Mo^0 (890 °C). [30-33] All peaks were slightly shifted from other reports because the reduction peak of catalysts depended on several factors such as preparation method and nickel doping effect. [33] However, the reduction band of Ni^{2+} to Ni^0 on H_2-TPR profile was not found at the low temperature range, i.e. 200-300 °C due to the weaker interaction between Ni^{2+} and Al_2O_3 around 200 °C. [33] Also, the small amount of Ni species in 19NiMo-Al catalyst led to the less H_2 consumption in good agreement with the smaller Ni^{+2} reduction band at high temperature compared with those of Mo reduction bands. The chemical species at the surface of the 19NiMo-Al catalyst were characterized by XPS technique. The Mo $3d_{5/2}$ peak was found at the binding energy around 233.2 eV (**Fig. 3)**, in the range of the oxidation state of Mo^{+6} in MoO_3 on the catalyst support (232.7 to 233.3 eV). [34, 35] The Ni $2p_{3/2}$ binding energy was shown ~855.2 eV which was close to Ni^{+2} in $NiMoO_4$ phases (855.2–857.2 eV). [34, 36]

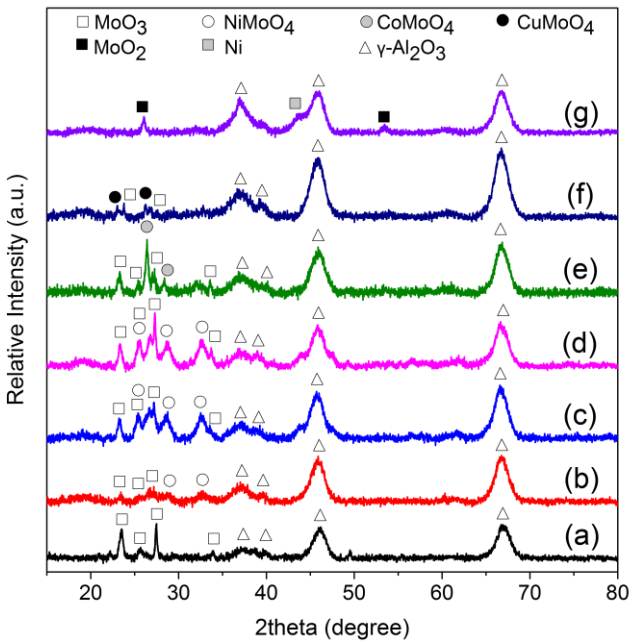

Fig. 1. Normalized XRD patterns of (a) 19Mo-Al, (b) 19NiMo-Al, (c) 27NiMo-Al, (d) 34NiMo-Al, (e) 19CoMo-Al, (f) 19CuMo-Al and (g) 19NiMo-Al (Red.).

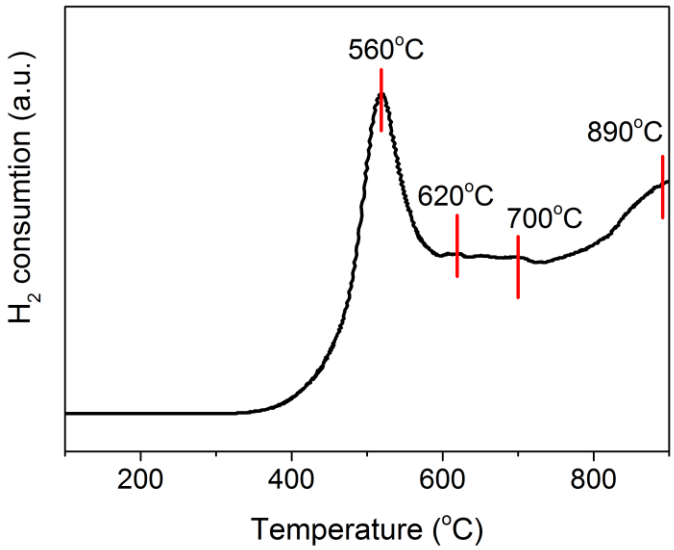

Fig. 2. The H_2-TPR profile of the 19NiMo-Al catalyst.

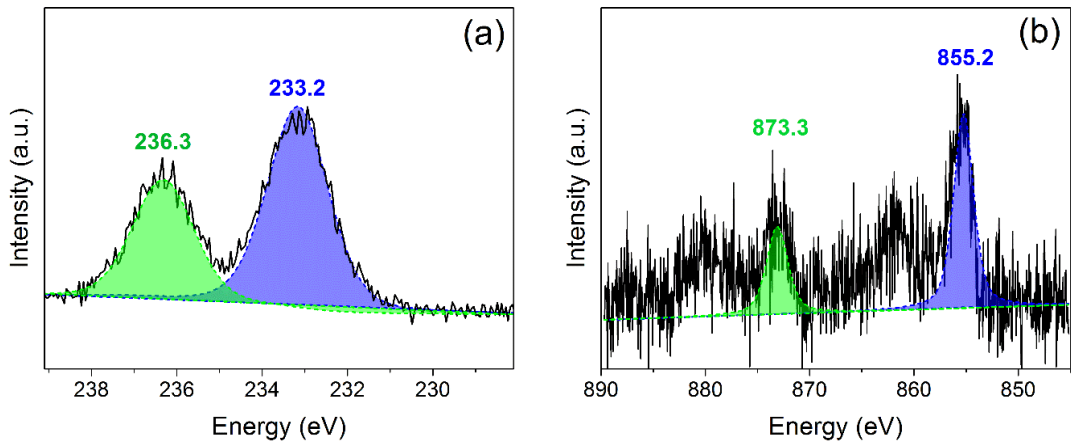

Fig. 3. XPS spectra of the 19NiMo-Al catalyst: (a) Mo 3d region (a) and (b) Ni 2p region.

The 19NiMo-Al catalyst was also analyzed by TEM technique to investigate the metal oxide morphology and dispersion. As shown in **Fig. 7**, the dark nanocrystals with a size in range of 5-10 nm represented metal oxides deposition which were well dispersed on the γ-Al_2O_3 support (gray elliptical nanocrystals). The BET specific surface area, total average pore volume and average pore diameter of all catalysts were listed in **Table 1**. The surface area of γ-Al_2O_3 was 255 m^2/g with total pore volume of 0.43 cc/g. The surface area of as-synthesized catalysts decreased by 12% after impregnation due to metal oxides coverage on γ-Al_2O_3. However, the blockage pores of catalysts

were not found apparently confirmed by the insignificant change in their pore volumes and pore size.

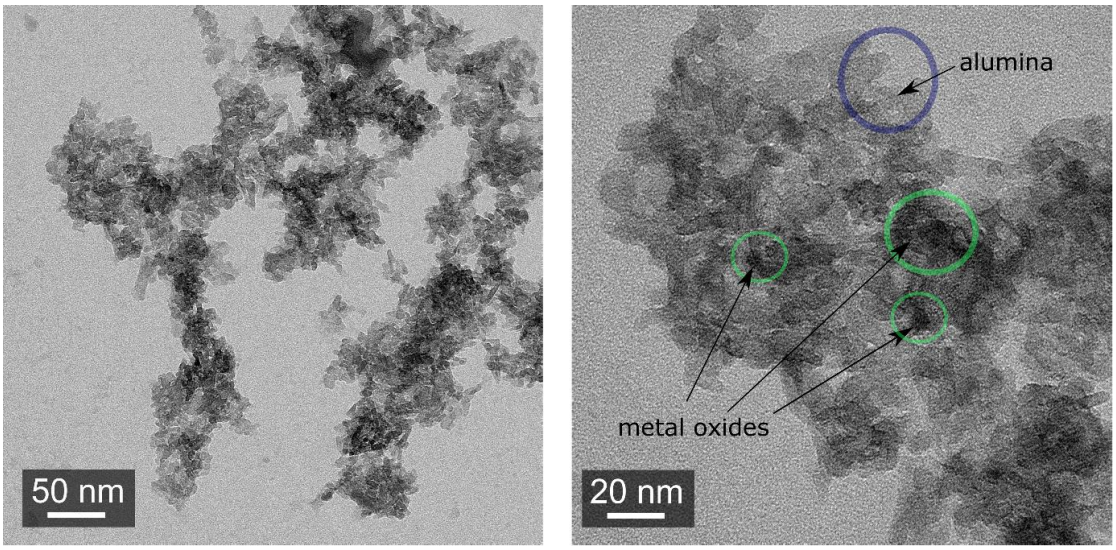

Fig. 7. TEM images of the 19NiMo-Al catalyst.

Table 1 Specific surface area and porous parameters of as-synthesized catalysts.

Catalyst	S_{BET} [a]	V_{total} [b]	d_p [b]
	m^2/g	cc/g	(nm)
γ-Alumina	209	0.577	7.8
19NiMo-Al	164	0.293	6.9
27NiMo-Al	137	0.311	6.9
34NiMo-Al	130	0.293	6.9
19Mo-Al	178	0.439	6.9
19CoMo-Al	167	0.403	7.7
19CuMo-Al	171	0.412	6.9

[a] Specific surface area calculated using the BET method

2.2. Deoxygenation of oleic acid

An oleic acid was used as a model compound to investigate deoxygenation behavior on MoO_3-based catalysts under various reaction conditions; gas atmosphere, pressure, temperature, and time. Shown in **Table 2**, all represented reactions using NiMo oxides/Al_2O_3 (19NiMo-Al) under N_2 atmosphere exhibited high %conversion in a

range of 70-90% with the highest at ~94% (condition 40N-350-6). For comparison, the reduced NiMo oxides/Al_2O_3, 19NiMo-Al (Red.) yielded lower %conversion (73.1%) than 19NiMo-Al (80.9%) did under the similar condition (40N-330-3). Thus, the NiMo oxides catalyst without the catalyst reduction pretreatment is highly active in the deoxygenation under N_2 pressure, suggesting that the oxide phases would play a crucial role in the deoxygenating reactions. This intensified process provided advantages over traditional deoxygenation under H_2 pressure. Additionally, the cooperation of Ni, Co, and Cu in MoO_3 showed the improvement of deoxygenation conversion in N_2 pressurization with the highest in the NiMo oxides catalyst. In case of the condition with H_2 atmosphere (condition 40H-330-3), the NiMo oxides catalyst showed 100% conversion; however, the product was yielded mostly in form of stearic acid without any desirable diesel-ranged hydrocarbon. Nevertheless, the stearic acid and saturated hydrocarbon were observed during deoxygenation of oleic acid under N_2 atmosphere as shown in **Fig. 8**. The results suggested that dehydrogenation and in-situ hydrogenation occurred as competitive reactions when using metal oxide catalysts. [37] Therefore, with these interesting results, we further studied in details of deoxygenation under inert atmosphere to optimize the hydrocarbon product yield.

Table 2 The catalytic performance of deoxygenation of oleic acid under various reaction conditions and catalysts.

Catalyst	Condition	Atmosphere	Pressure (bar)	Temperature (°C)	Time (hour)	%conversion
19NiMo-Al	40H-330-3	H_2	40	330	3	100.0
19NiMo-Al	10N-330-3	N_2	10	330	3	77.1
19NiMo-Al	40N-330-3	N_2	40	330	3	80.9
27NiMo-Al	40N-330-3	N_2	40	330	3	74.0
34NiMo-Al	40N-330-3	N_2	40	330	3	67.3
19NiMo-Al	40N-300-3	N_2	40	300	3	43.5
19NiMo-Al	40N-350-3	N_2	40	350	3	84.7
19NiMo-Al	40N-330-6	N_2	40	330	6	86.2
19NiMo-Al	40N-330-9	N_2	40	330	9	89.6
19NiMo-Al	40N-350-6	N_2	40	350	6	94.1
19Mo-Al	40N-330-3	N_2	40	330	3	67.5
19CoMo-Al	40N-330-3	N_2	40	330	3	74.6
19CuMo-Al	40N-330-3	N_2	40	330	3	72.3
19NiMo-Al (red)	40N-330-3	N_2	40	330	3	73.3

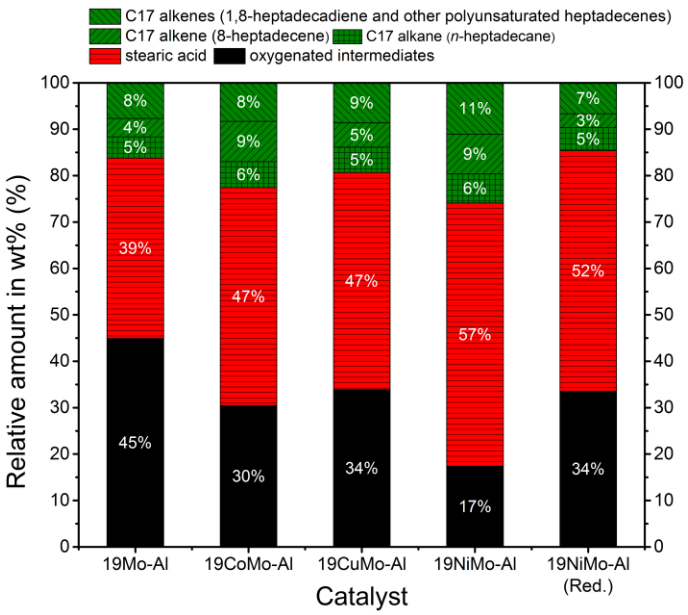

Fig. 8. Liquid product distribution obtained by deoxygenation of oleic acid using MoO_3-based catalysts under the reaction condition of 330°C, 3 h, and N_2 pressure of 40 bar.

The liquid product distributions in **Fig.8** showed that the monometal oxide catalyst, 19Mo-Al, exhibited lower C17 hydrocarbons yield (the target products) than bimetal oxide catalysts on alumina. The NiMo oxides catalyst achieved the highest C17 hydrocarbons yield compared with the reduced NiMo, CoMo oxides, and CuMo oxides. Furthermore, the intermediates found in all cases were notable stearic acid and other oxygenated compounds such as long-chain alcohols. Demonstrated in **Fig. 8**, the 19NiMo-Al yielded the more amount of stearic acid and lower oxygenated products suggesting that the Ni-doped molybdenum oxide catalysts with the MoO_3 and $NiMoO_4$ as active phases could promote dehydrogenation in N_2 atmosphere and obtained readily hydrogen species which was subsequently hydrogenated the nearby oleic acid molecules (unsaturated fatty acid) to generate stearic acid (saturated fatty acid). Besides, the reduced NiMo oxides (19NiMo-Al (Red.)) did not show a good catalytic activity in the inert atmosphere. Perhaps, the MoO_2 and Ni metal (Ni^0) as active phases in this catalyst could be working in the high concentration of H_2 gas and also being an ineffective dehydrogenation catalyst. [37] The CO_2 and CO gas products in the reaction were found notably without any trace of H_2 suggesting the DCO_2 and DCO of oleic acid as the main pathways of deoxygenation under N_2 pressure to produce C17 hydrocarbons. The influence of the metal loading (19, 27, and 34 wt%.) on deoxygenation performance was studied at 330°C for 3 h under N_2 pressure of 40 bar (condition 40N-330-3). As demonstrated in **Table 1** and **Fig.9**, the conversion and liquid product distribution of C17 hydrocarbons trended to decrease when increasing the metal

loading from 19% to 34% because the large amount of metal oxides coverage on alumina leaded to significant decrease in surface area and pore volume of catalysts. Additionally, over NiMo oxides catalyst, changing N_2 pressure from 10 to 40 bar did not significantly affect the deoxygenation performance due to only a slight change (in several percentage) of conversion) and product yield (**Fig. 10**).

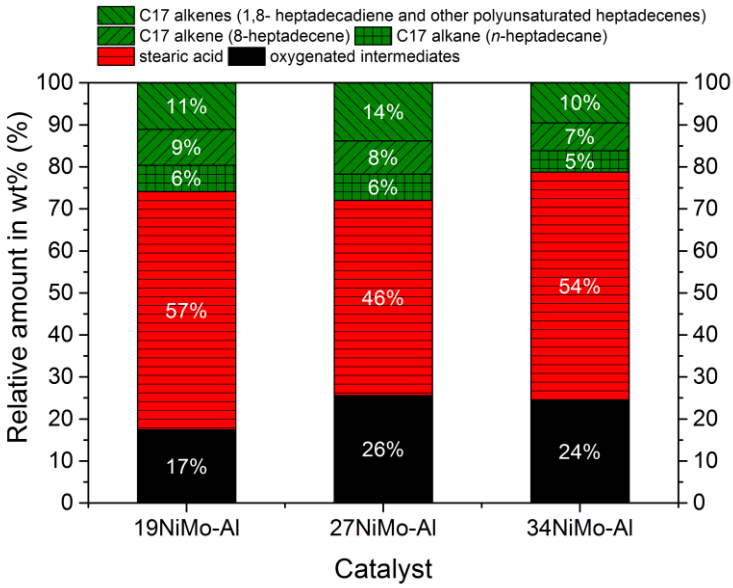

Fig. 9. Liquid product distribution obtained by deoxygenation of oleic acid using different metal loading on NiMo oxides/γ-Al_2O_3 catalysts under the reaction condition of 330°C, 3 h, and N_2 pressure of 40 bar.

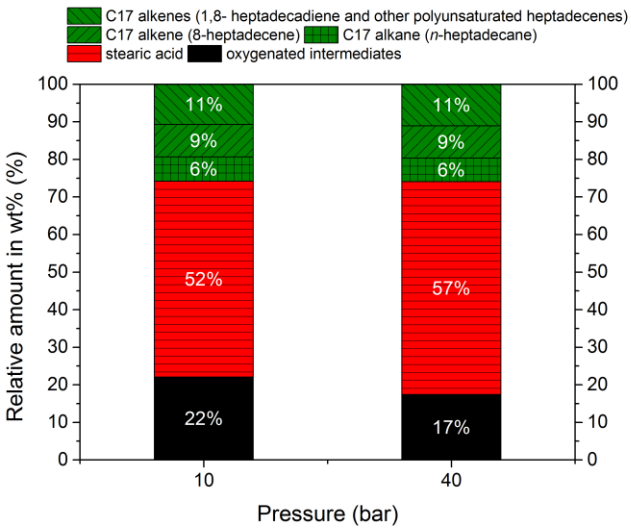

Fig. 10. Liquid product distribution obtained by deoxygenation of oleic acid using 19NiMo-Al catalyst under the reaction condition of 330°C, 3 h, and N_2 pressure of 10-40 bar.

The raising of reaction time during deoxygenation under N_2 atmosphere from 3 to 9 h showed the improvement of oleic acid conversion from 80.9% to 89.6% as well as their C17 hydrocarbons and intermediates (**Fig. 11**). Furthermore, the increase of reaction time from 3 to 6 h resulted in lower amount of stearic acid because the DCO_2 and/or DCO of stearic acid could subsequently occur. The amount of stearic acid did not change significantly at time interval of 6 to 9 h, showing that is the hydrogenation rate of oleic acid and deoxygenation rate of stearic acid would be comparable under this condition. The variation of reaction temperature showed high impact on deoxygenation of oleic acid under N_2 pressure resulting in the enhancement of conversion, from 43.5% at 300°C to 84.7% at 350°C, and C17 hydrocarbons yield which raised over 25% (**Fig. 12**). On the other hand, the stearic acid was still detected at the reaction temperature range of 300-350 °C under N_2 gas indicating the presences of dehydrogenation with subsequently hydrogenation as side reactions as previously discussed. Moreover, the C8-C16 hydrocarbons and hydrocarbon gases (C1-C3) were observed at high deoxygenation temperature since 330 °C due to thermal cracking reaction and those product amounts increased at 350 °C with prolonged reaction time from 3 to 6 h as shown in **Fig. 13**.

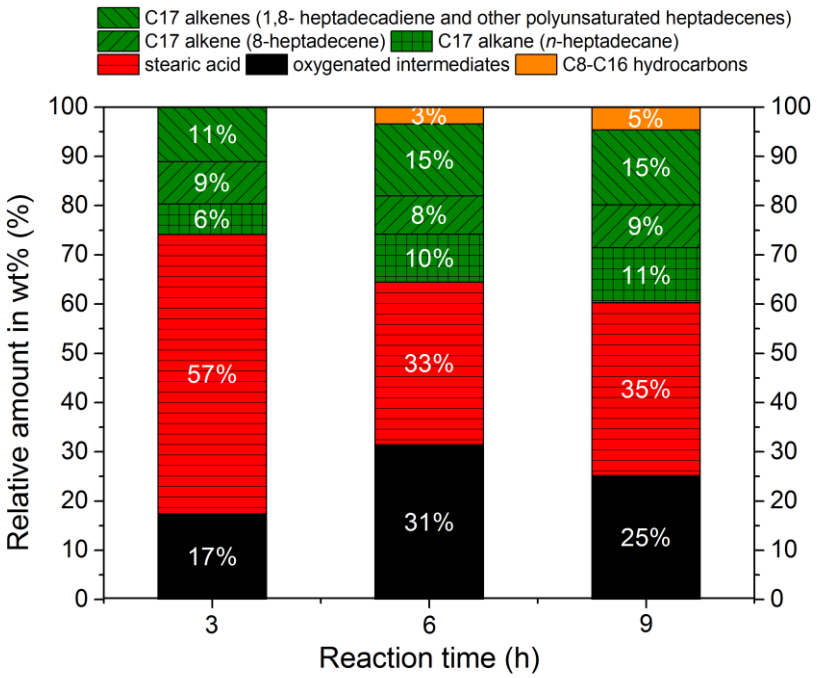

Fig. 11. Liquid product distribution obtained by deoxygenation of oleic acid using 19NiMo-Al catalyst under the reaction condition of 330°C, 3-9 h, and N_2 pressure of 40 bar.

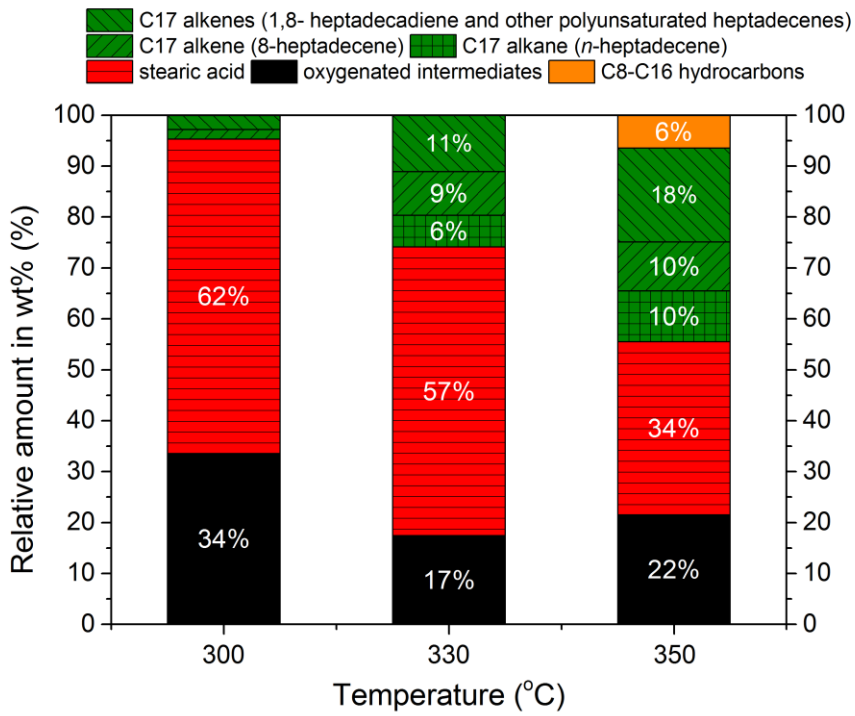

Fig. 12. Liquid product distribution obtained by deoxygenation of oleic acid using 19NiMo-Al catalyst under the reaction condition of 300-350°C, 3 h, and N_2 pressure of 40 bar.

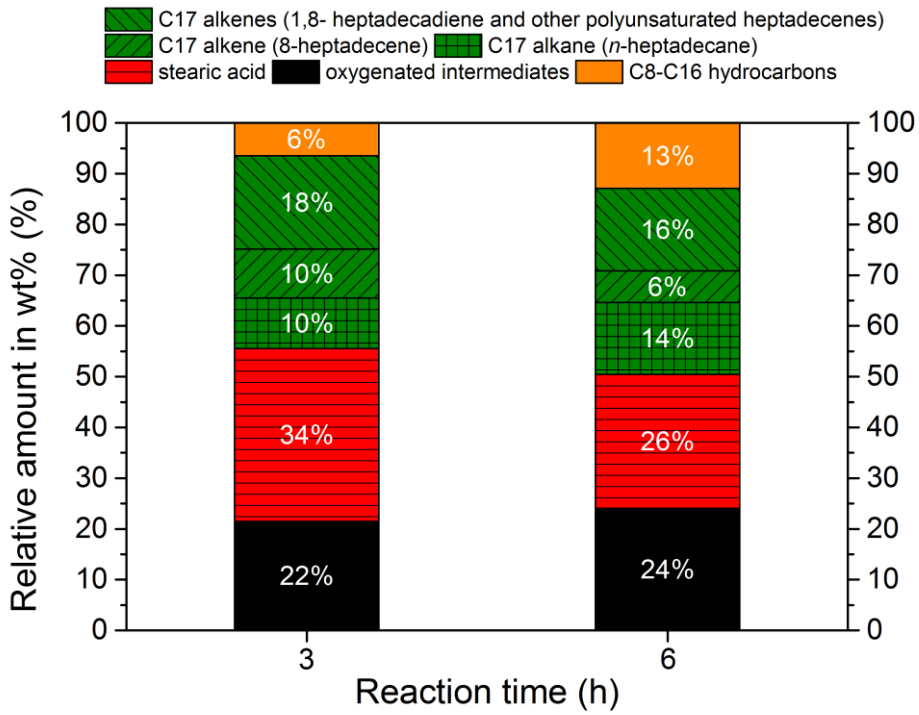

Fig. 13. Liquid product distribution obtained by deoxygenation of oleic acid using 19NiMo-Al catalyst under the reaction condition of 350°C, 3-6 h, and N_2 pressure of 40 bar.

3. Conclusion

The deoxygenation of oleic acid for producing diesel-ranged hydrocarbon was investigated over MoO_3-based catalysts with Ni, Co, and Cu cooperation prepared by wetness impregnation. The as-synthesized catalysts exhibited the well-dispersion of metal oxide phases, MoO_3 and $XMoO_4$ (X = Ni, Co, Cu), on alumina evaluated by SEM-EDX mapping and electron back-scattering imaging. The NiMo oxides/γ-Al_2O_3 (containing MoO_3 and $NiMoO_4$ phases) exhibited the highest deoxygenation performance, compared with those of supported MoO_3, CoMo oxides, and CuMo oxides, with the conversion over 80% under N_2 atmosphere and good selectivity of C17 alkenes in liquid product. On the other hand, the reduced NiMo oxides/γ-Al_2O_3 catalyst containing MoO_2 and Ni (0) phases showed the lower catalytic activity under inert atmosphere in comparison to the non-reduced ones. The rising of reaction time and temperature enhance the conversion and selectivity of desired C17 hydrocarbon products; nevertheless, the thermal cracking at too high temperature i.e. 350 ^{o}C occurred as well and decreased the C17 hydrocarbons yield. The highest conversion was obtained over 94% with 36% C17 hydrocarbons at 350 ^{o}C, 6 h under N_2 pressure of 40 bar using 19%NiMo oxides/γ-Al_2O_3 catalyst. The deoxygenation pathway under N_2 pressure was proposed via decarbonylation and decarboxylation. However, the noticeable amount of stearic acid (saturated fatty acid) was also detected as well as n-heptadecane (saturated C17 hydrocarbons) indicating the in-situ active hydrogen sources possibly generated from dehydrogenation as a side reaction which was evidenced by the production of polyunsaturated heptadecene.

References

[1] V.T. da Silva, L.A. Sousa, Chapter 3 - Catalytic Upgrading of Fats and Vegetable Oils for the Production of Fuels A2 - Triantafyllidis, Kostas S, in: A.A. Lappas, M. Stöcker (Eds.) The Role of Catalysis for the Sustainable Production of Bio-fuels and Bio-chemicals, Elsevier, Amsterdam, 2013, pp. 67-92.

[2] C.-C. Liu, W.-C. Lu, T.-J. Liu, Transesterification of Soybean Oil Using CsF/CaO Catalysts, Energy Fuels, 26 (2012) 5400-5407.

[3] S. Nasreen, H. Liu, L.A. Qureshi, Z. Sissou, I. Lukic, D. Skala, Cerium–manganese oxide as catalyst for transesterification of soybean oil with subcritical methanol, Fuel Process. Technol., 148 (2016) 76-84.

[4] J.V. Gerpen, Biodiesel processing and production, Fuel Process. Technol., 86 (2005) 1097-1107.

[5] J.G. Immer, M.J. Kelly, H.H. Lamb, Catalytic reaction pathways in liquid-phase deoxygenation of C18 free fatty acids, Appl. Catal., A, 375 (2010) 134-139.

[6] A.M.A. Attia, A.E. Hassaneen, Influence of diesel fuel blended with biodiesel produced from waste cooking oil on diesel engine performance, Fuel, 167 (2016) 316-328.

[7] L. Hermida, A.Z. Abdullah, A.R. Mohamed, Deoxygenation of fatty acid to produce diesel-like hydrocarbons: A review of process conditions, reaction kinetics and mechanism, Renewable and Sustainable Energy Reviews, 42 (2015) 1223-1233.

[8] A.T. Madsen, B. Rozmysłowicz, I.L. Simakova, T. Kilpiö, A.-R. Leino, K. Kordás, K. Eränen, P. Mäki-Arvela, D.Y. Murzin, Step Changes and Deactivation Behavior in the Continuous Decarboxylation of Stearic Acid, Ind. Eng. Chem. Res., 50 (2011) 11049-11058.

[9] M. Snåre, I. Kubičková, P. Mäki-Arvela, K. Eränen, D.Y. Murzin, Heterogeneous catalytic deoxygenation of stearic acid for production of biodiesel, Ind. Eng. Chem. Res., 45 (2006) 5708-5715.

[10] N.A. Grosso-Giordano, T.R. Eaton, Z. Bo, S. Yacob, C.-C. Yang, J.M. Notestein, Silica support modifications to enhance Pd-catalyzed deoxygenation of stearic acid, Appl. Catal., B, 192 (2016) 93-100.

[11] T. Li, J. Cheng, R. Huang, J. Zhou, K. Cen, Conversion of waste cooking oil to jet biofuel with nickel-based mesoporous zeolite Y catalyst, Bioresour. Technol., 197 (2015) 289-294.

[12] C. Zhao, W. Song, J.A. Lercher, Aqueous Phase Hydroalkylation and Hydrodeoxygenation of Phenol by Dual Functional Catalysts Comprised of Pd/C and H/La-BEA, ACS Catal., 2 (2012) 2714-2723.

[13] K. Sun, A.R. Wilson, S.T. Thompson, H.H. Lamb, Catalytic Deoxygenation of Octanoic Acid over Supported Palladium: Effects of Particle Size and Alloying with Gold, ACS Catal., 5 (2015) 1939-1948.

[14] A. Srifa, K. Faungnawakij, V. Itthibenchapong, N. Viriya-empikul, T. Charinpanitkul, S. Assabumrungrat, Production of bio-hydrogenated diesel by catalytic hydrotreating of palm oil over NiMoS2/γ-Al2O3 catalyst, Bioresour. Technol., 158 (2014) 81-90.

[15] O.İ. Şenol, T.R. Viljava, A.O.I. Krause, Hydrodeoxygenation of methyl esters on sulphided NiMo/γ-Al2O3 and CoMo/γ-Al2O3 catalysts, Catal. Today, 100 (2005) 331-335.

[16] V. Itthibenchapong, A. Srifa, R. Kaewmeesri, P. Kidkhunthod, K. Faungnawakij, Deoxygenation of palm kernel oil to jet fuel-like hydrocarbons using Ni-MoS2/γ-Al2O3 catalysts, Energy Convers. Manage., 134 (2017) 188-196.

[17] L. Yang, K.L. Tate, J.B. Jasinski, M.A. Carreon, Decarboxylation of Oleic Acid to Heptadecane over Pt Supported on Zeolite 5A Beads, ACS Catal., 5 (2015) 6497-6502.

[18] M. Ahmadi, A. Nambo, J.B. Jasinski, P. Ratnasamy, M.A. Carreon, Decarboxylation of oleic acid over Pt catalysts supported on small-pore zeolites and hydrotalcite, Catal. Sci. Technol., 5 (2015) 380-388.

[19] J.A. Lopez-Ruiz, R.J. Davis, Decarbonylation of heptanoic acid over carbon-supported platinum nanoparticles, Green Chem., 16 (2014) 683-694.

[20] J. Liu, F.R. Lucci, M. Yang, S. Lee, M.D. Marcinkowski, A.J. Therrien, C.T. Williams, E.C. Sykes, M. Flytzani-Stephanopoulos, Tackling CO Poisoning with Single-Atom Alloy Catalysts, J. Am. Chem. Soc., 138 (2016) 6396-6399.

[21] M. Guisnet, P. Magnoux, Organic chemistry of coke formation, Appl. Catal., A, 212 (2001) 83-96.

[22] T. Yeh, S. Linic, P.E. Savage, Deactivation of Pt catalysts during hydrothermal decarboxylation of butyric acid, ACS Sus. Chem. Eng., 2 (2014) 2399-2406.

[23] C.H. Bartholomew, Mechanisms of catalyst deactivation, Appl. Catal., A, 212 (2001) 17-60.

[24] E. Laurent, B. Delmon, Influence of water in the deactivation of a sulfided NiMoγ-Al2O3 catalyst during hydrodeoxygenation, J. Catal., 146 (1994) 281-291.

[25] T.R. Viljava, R.S. Komulainen, A.O.I. Krause, Effect of H2S on the stability of CoMo/Al2O3 catalysts during hydrodeoxygenation, Catal. Today, 60 (2000) 83-92.

[26] J.A. Botas, D.P. Serrano, A. García, J. de Vicente, R. Ramos, Catalytic conversion of rapeseed oil into raw chemicals and fuels over Ni- and Mo-modified nanocrystalline ZSM-5 zeolite, Catal. Today, 195 (2012) 59-70.

[27] N. Chen, S. Gong, E.W. Qian, Effect of reduction temperature of NiMoO3-x/SAPO-11 on its catalytic activity in hydrodeoxygenation of methyl laurate, Appl. Catal., B, 174-175 (2015) 253-263.

[28] T. Prasomsri, M. Shetty, K. Murugappan, Y. Roman-Leshkov, Insights into the catalytic activity and surface modification of MoO3 during the hydrodeoxygenation of lignin-derived model compounds into aromatic hydrocarbons under low hydrogen pressures, Energy Environ. Sci., 7 (2014) 2660-2669.

[29] T. Prasomsri, T. Nimmanwudipong, Y. Roman-Leshkov, Effective hydrodeoxygenation of biomass-derived oxygenates into unsaturated hydrocarbons by MoO3 using low H2 pressures, Energy Environ. Sci., 6 (2013) 1732-1738.

[30] L. Kaluža, R. Palcheva, A. Spojakina, K. Jirátová, G. Tyuliev, Hydrodesulfurization NiMo catalysts supported on Co, Ni and B modified Al2O3 from Anderson heteropolymolybdates, Procedia Engineering, 42 (2012) 873-884.

[31] Y. Meng, T. Wang, S. Chen, Y. Zhao, X. Ma, J. Gong, Selective oxidation of methanol to dimethoxymethane on V2O5–MoO3/γ-Al2O3 catalysts, Appl. Catal., B, 160–161 (2014) 161-172.

[32] R. Singh, D. Kunzru, Hydrodesulfurization of dibenzothiophene on NiMo/γ-Al2O3 washcoated monoliths, Fuel, 163 (2016) 180-188.

[33] M.H. Youn, J.G. Seo, P. Kim, I.K. Song, Role and effect of molybdenum on the performance of Ni-Mo/gamma-Al2O3 catalysts in the hydrogen production by auto-thermal reforming of ethanol, Journal of Molecular Catalysis A-Chemical, 261 (2007) 276-281.

[34] D. Nikolova, R. Edreva-Kardjieva, G. Gouliev, T. Grozeva, P. Tzvetkov, The state of (K)(Ni)Mo/γ-Al2O3 catalysts after water–gas shift reaction in the presence of sulfur in the feed: XPS and EPR study, Appl. Catal., A, 297 (2006) 135-144.

[35] A.A. Smirnov, S.A. Khromova, D.Y. Ermakov, O.A. Bulavchenko, A.A. Saraev, P.V. Aleksandrov, V.V. Kaichev, V.A. Yakovlev, The composition of Ni-Mo phases obtained by NiMoOx-SiO2 reduction and their catalytic properties in anisole hydrogenation, Appl. Catal., A, 514 (2016) 224-234.

[36] P. Dufresne, E. Payen, J. Grimblot, J.P. Bonnelle, Study of nickel-molybdenum-.gamma.-aluminum oxide catalysts by x-ray photoelectron and Raman spectroscopy. Comparison with cobalt-molybdenum-.gamma.-aluminum oxide catalysts, The Journal of Physical Chemistry, 85 (1981) 2344-2351.

[37] J.J.H.B. Sattler, J. Ruiz-Martinez, E. Santillan-Jimenez, B.M. Weckhuysen, Catalytic Dehydrogenation of Light Alkanes on Metals and Metal Oxides, Chem. Rev., 114 (2014) 10613-10653.

[38] D. Kubička, L. Kaluža, Deoxygenation of vegetable oils over sulfided Ni, Mo and NiMo catalysts, Appl. Catal., A, 372 (2010) 199-208.

[39] C. Wang, Q. Liu, J. Song, W. Li, P. Li, R. Xu, H. Ma, Z. Tian, High quality diesel-range alkanes production via a single-step hydrotreatment of vegetable oil over Ni/zeolite catalyst, Catal. Today, 234 (2014) 153-160.

[40] K. Chen, S. Xie, A.T. Bell, E. Iglesia, Structure and Properties of Oxidative Dehydrogenation Catalysts Based on MoO3/Al2O3, J. Catal., 198 (2001) 232-242.

[41] B. Pillay, M.R. Mathebula, H.B. Friedrich, The oxidative dehydrogenation of n-hexane over Ni–Mo–O catalysts, Appl. Catal., A, 361 (2009) 57-64.

[42] P. ŠimáČek, D. KubiČka, G. Šebor, M. Pospíšil, Hydroprocessed rapeseed oil as a source of hydrocarbon-based biodiesel, Fuel, 88 (2009) 456-460.

[43] M. Yang, B. Han, H. Cheng, First-Principles Study of Hydrogenation of Ethylene on a HxMoO3(010) Surface, The Journal of Physical Chemistry C, 116 (2012) 24630-24638.

[44] Y.-H. Lei, Z.-X. Chen, DFT+U Study of Properties of MoO3 and Hydrogen Adsorption on MoO3(010), The Journal of Physical Chemistry C, 116 (2012) 25757-25764.

Deoxygenation of Stearic acid into to diesel-range hydrocarbon using NiSn catalysts

1. *Experimental*

The Ni/γ-Al_2O_3 and NiSn/γ-Al_2O_3 catalysts were prepared by wetness impregnation with metal precursor solution using nickel nitrate hexahydrate ($Ni(NO_3)_2 \cdot 6H_2O$, Sigma-Aldrich, 98.8%), $SnCl_2 \cdot 2H_2O$ (Carlo Erba, 99.0%), and spherical γ-Al_2O_3 (1.8 mm of O.D., Sasol Company) as the support. The Ni loading was constantly 18 wt.%, while Sn loading was varied between 0.5-7 wt.%. The impregnated catalysts were dried overnight at 100 ^oC in an oven before calcination at 500^oC for 5 h in static air. Prior catalytic testing, the catalysts were reduced at 500 ^oC for 4 h in H_2 gas flow (50 mL/min). Phase identity of the catalyst was analyzed by X-ray diffraction (XRD) using a Bruker D8 Advance with Cu Kα radiation. The measurement was carried out at 40 kV and 40 mA and over a range of 10°<2theta<80°, 0.02 deg s^{-1} increment with a step time of 1 s). The chemical state at the surface of the catalyst was analyzed by X-ray photoelectron spectroscopy (XPS) using PHI 5000 Versa Probe II XPS (ULVAC-PHI). The Brunauer–Emmett–Teller (BET) surface area and Barrett-Joyner-Halenda (BJH) pore size of the catalysts were investigated by a N_2 sorption analyzer (Quanta Chrome NOVA2000e).

Deoxygenation reactions were carried out in a 300 mL of Parr 4568 batch reactor. A steric acid (Aldrich, technical grade, 90% purity) was used as a model compound of palm oil without further purification. Typically, a 5 g of stearic acid was dissolved in 40 mL of dodecane, then the solution was transferred to the reactor. The spherical Ni/Al_2O_3 or NiSn/ Al_2O_3 catalyst loading of 20% w/w of reactant, i.e. 1 g of catalyst and 5 g of stearic acid, was introduced in the reactor. The reaction testing was performed under these conditions: 40 bar of H_2 pressurizing at room temperature, stirring rate of 500 rpm, reaction temperature of 300 to 340 ^oC, and reaction time of 1 to 9 h. Liquid products were analyzed by a GC-MS (Agilent Technologies, 7890A) and a GC-FID (GC-2014, Shimadzu) equipped with DB-1HT columns (30m x 0.32mm x 0.1μm). The gas products were analyzed by a GC-TCD (Shimadzu GC2010plus) equipped with MS13X and Porapak Q columns.

2. *Results and discussion*

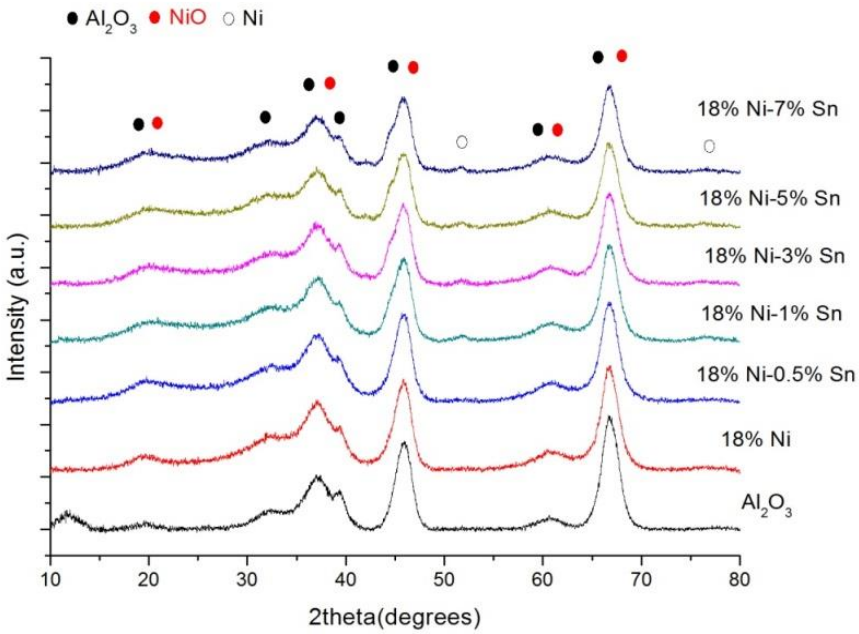

Fig. 1 The XRD patterns of NiSn catalysts.

The NiSn catalysts were prepared with constant 18 wt.%Ni and vary Sn doping in a range of 0.5-7 wt.%. Demonstrated in **Fig. 1,** the Ni metal phase (open circle) was detected in every samples, while the Sn peaks were not clearly found in the patterns. However, the XPS techniques (**Table 1**) revealed the surface species of catalyst containing Ni and Sn in both metal and oxide phases; therefore, the Sn doping in Ni catalysts was confirmed. The SnO_2 (Sn^{4+}) phase was not completely reduced to Sn metal phase at 500 ^{o}C in H_2 flow as found partial reduction to SnO (Sn^{2+}) referring the strong Sn-O bonding nature compared with Ni-O bonding.

The BET specific surface area, total average pore volume and average pore diameter of all catalysts were listed in **Table 2**. The surface area of γ-Al_2O_3 was 211 m^2/g with total pore volume of 0.573 cc/g. The surface area of NiSn catalysts slightly decreased after impregnation, calcination, and H_2-reduction due to metal coverage on γ-Al_2O_3. However, the blockage pores of catalysts were not found apparently confirmed by the insignificant change in their pore volumes and pore size.

Table 1 Surface species of NiSn catalysts analyzed by XPS.

Catalyst	Ni species	Sn species
18wt%Ni-**0.5wt%Sn/Al_2O_3**	$2p_{3/2}$ $Ni(OH)_2$ $2p_{3/2}$, satellite $2p_{1/2}$ $Ni(OH)_2$ $2p_{1/2}$, satellite	$3d_{5/2}$ SnO_2 $3d_{3/2}$ SnO_2
18wt%Ni-**7wt%Sn/Al_2O_3**		
18wt%Ni-**0.5wt%Sn/Al_2O_3** (reduced)	$2p_{3/2}$NiO $2p_{3/2}$, satellite $2p_{1/2}$ NiO $2p_{1/2}$, satellite	$3d_{5/2}$ SnO $3d_{3/2}$ SnO
18wt%Ni-**3wt%Sn/Al_2O_3** (reduced)	$2p_{3/2}$ Ni $2p_{1/2}$ Ni $2p_{3/2}$NiO $2p_{3/2}$, satellite $2p_{1/2}$ NiO $2p_{1/2}$, satellite	$3d_{5/2}$ Sn $3d_{3/2}$ $3d_{5/2}$ SnO $3d_{3/2}$ SnO
18wt%Ni-**7wt%Sn/Al_2O_3** (reduced)		

A stearic acid was used as a model compound to investigate deoxygenation behavior on NiSn catalysts under hydrogen pressure (40 bar) with reaction temperature of 300 ^{o}C for 1 h. Shown in **Fig. 2** and **Fig. 3**, the conversion of stearic acid and alkanes selectivity apparently deceased when using high concentration of Sn (1-7%). The decarboxylation and decarbonylation remained the main pathway of deoxygenation when using Ni and NiSn catalysts indicated by the high selectivity of C17 alkane (heptadecane) over C18 alkane (octadecane). In addition, a C36 product as a side product identified as C36 via GC-MS was detected with high selectivity in case of high Sn doping in Ni catalysts, thus the Sn doping could change the reaction from deoxygenation to others e.g. esterification or polymerization.

Table 2 Specific surface area and porous parameters of Ni and NiSn catalysts.

Sample	Surface Area (m^2/g)	Pore Volume (cc/g)	Pore Diameter (nm)
γ-Al_2O_3	211	0.573	7.8
18wt%Ni/Al_2O_3	182	0.532	7.8
18wt%Ni-0.5wt%Sn	193	0.556	7.8
18wt%Ni-1wt%Sn	184	0.507	7.8
18wt%Ni-3wt%Sn	187	0.546	7.8
18wt%Ni-5wt%Sn	190	0.541	7.8
18wt%Ni-7wt%Sn	191	0.524	7.8

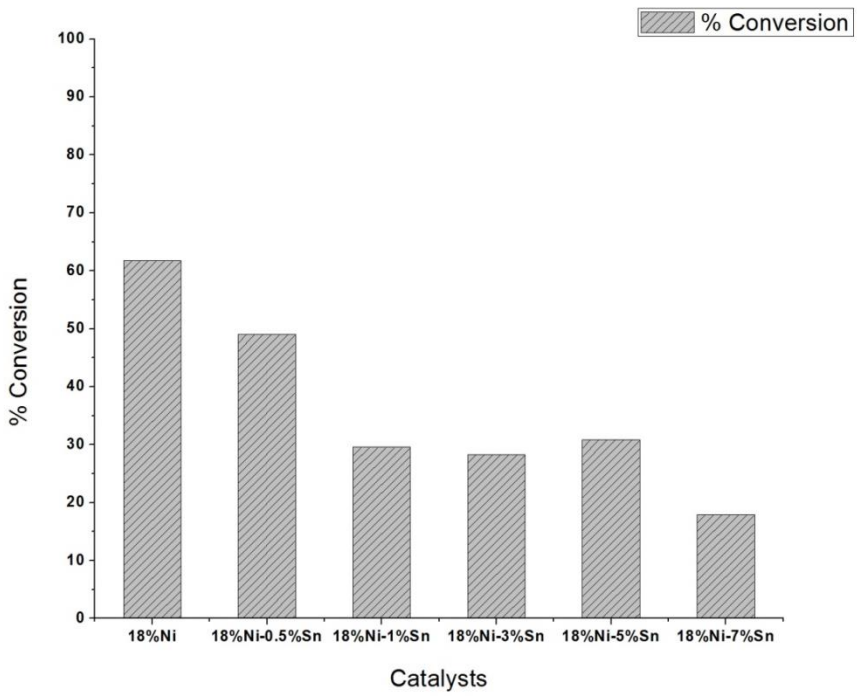

Fig. 2 stearic acid conversion comparison when using NiSn catalysts. The reaction testing was performed under 40-bar H_2 pressure, reaction temperature of 300 ^{o}C for 1h.

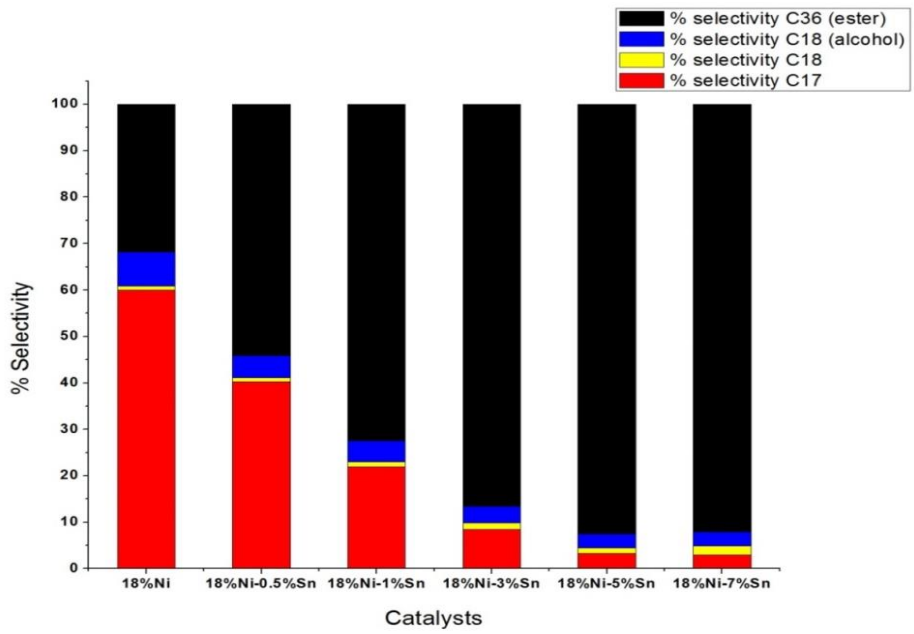

Fig 3 product selectivity comparison when using of NiSn catalysts. The reaction testing was performed under 40-bar H_2 pressure, reaction temperature of 300 ^{o}C for 1 h.

When increasing both reaction temperature (300 to 340 ^{o}C; the result was not shown) and reaction time (1 to 6 h), the NiSn (0.5 wt.%Sn) catalyst showed catalytic performance similarly to the Ni catalyst in the first-time usage and become higher in the several using indicating the higher stability as shown in **Fig. 4**, while the Ni catalyst deactivation occurred much faster and clearly seen at the fourth cycle as the significant decrease in both conversion and selectivity in comparison to those of NiSn catalyst.

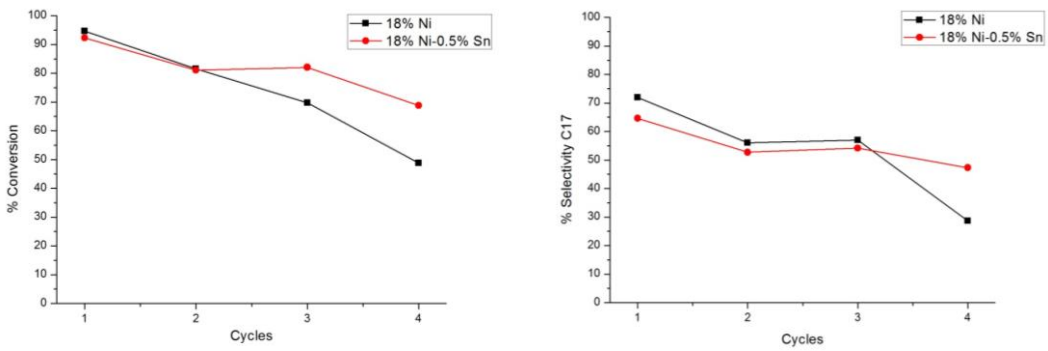

Fig. 4 stearic acid conversion and hetadecane selectivity comparison when using 18 wt.% Ni/Al_2O_3 and 18 wt.%Ni0.5 wt.%Sn $/Al_2O_3$ catalysts. Each cycle was performed under 40-bar H_2 pressure, reaction temperature of 300 ^{o}C for 6 h.

3. *Conclusion*

Deoxygenation of fatty acid molecules has been employed as one of promising processes for highly efficient production of renewable diesel. In addition, non-noble metal catalysts e.g. Ni, Co, Cu have become attractive as an alternative low cost material group and to avoid sulfur contamination in fuel product compared with the conventional $NiMoS_2$ and $CoMoS_2$ catalysts. In this work, the Ni/γ-Al_2O_3 and NiSn/γ-Al_2O_3 catalysts were prepared by wetness impregnation method and characterized by various techniques. The decarboxylation and decarbonylation of stearic acid to produce heptadecane ($C_{17}H_{36}$) were proposed as the main pathways over the use of NiSn catalysts, whereas the hydrodeoxygenation (HDO) became a minor reaction confirmed by the high selectivity of C17 over C18 alkanes. The concentration of Sn doped in Ni catalyst apparently affected the stearic acid conversion and selectivity of hydrocarbon products. Moreover, Sn doping apparently improved Ni catalyst stability and extend catalyst life time and reusability; perhaps by reducing coke formation on the Ni surface.

Suggestion for future research

- Exploration of novel catalysts with high deoxygenation performance under low hydrogen pressure condition can reduce cost effective in biofuel production from biomass feedstock and expand vastly utilization of this technology in the industry segment.
- Kinetic reaction study could provide the useful information for both fundamental and applied research and encourage the outstanding publication in high impact journals.
- Computational simulation combined with experimental results will be useful to explain chemical reaction mechanism in certain catalyst surface structure.

Output จากโครงการวิจัยที่ได้รับทุนจาก สกว.

1. ผลงานตีพิมพ์ในวารสารวิชาการนานาชาติ (ระบุชื่อผู้แต่ง ชื่อเรื่อง ชื่อวารสาร ปี เล่มที่ เลขที่ และหน้า) หรือผลงานตามที่คาดไว้ในสัญญาโครงการ

1.1 **Vorranutch Itthibenchapong**, Atthapon Srifa, Rungnapa Kaewmeesri, Pinit Kidkhunthod, Kajornsak Faungnawakij*, Deoxygenation of palm kernel oil to jet fuel-like hydrocarbons using Ni-MoS_2/γ-Al_2O_3 catalysts, Energy Conversion and Management, 2017, 134,188-196.

1.2 Navapat Krobkrong, **Vorranutch Itthibenchapong***, Pipat Khongpracha, Kajornsak Faungnawakij, Deoxygenation of oleic acid under an inert atmosphere using molybdenum oxide-based catalysts. (Manuscript submission)

2. การนำผลงานวิจัยไปใช้ประโยชน์
   - เชิงพาณิชย์ (มีการนำไปผลิต/ขาย/ก่อให้เกิดรายได้ หรือมีการนำไปประยุกต์ใช้โดยภาคธุรกิจ/บุคคลทั่วไป)
   - เชิงนโยบาย (มีการกำหนดนโยบายอิงงานวิจัย/เกิดมาตรการใหม่/เปลี่ยนแปลงระเบียบข้อบังคับหรือวิธีทำงาน)
   - เชิงสาธารณะ (มีเครือข่ายความร่วมมือ/สร้างกระแสความสนใจในวงกว้าง)
   - เชิงวิชาการ (มีการพัฒนาการเรียนการสอน/สร้างนักวิจัยใหม่)
3. อื่นๆ (เช่น ผลงานตีพิมพ์ในวารสารวิชาการในประเทศ การเสนอผลงานในที่ประชุมวิชาการ หนังสือ การจดสิทธิบัตร)

3.1 **Vorranutch Itthibenchapong**, Atthapon Srifa, Kajornsak Faungnawakij, Chapter 11 Heterogeneous Catalysts for Advanced Biofuel Production, Nanotechnology for Bioenergy and Biofuel Production, 2017, 1st Ed., Print ISBN 978-3-319-45458-0, Online ISBN 978-3-319-45459-7. E-book publishing: December 2016. (International book chapter)

3.2 **Vorranutch Itthibenchapong***, Navapat Krobkrong, Kajornsak Faungnawakij, Development of Nanostructured Metal Oxide Catalysts for Advanced Biofuel Production, The 24th European Biomass Conference & Exhibition (EUBCE 2016), 6-9 June 2016, Amsterdam, Netherland. (conference poster presentation)

3.3 Navapat Krobkrong, **Vorranutch Itthibenchapong***, Pipat Khongpracha, Efficiency of Nickel molybdenum oxide on alumina supported during catalytic deoxygenation of fatty acid under inert atmosphere, PACCON 2016, 9-11 February 2016, Bangkok Thailand. (conference oral presentation abstract)

3.4 Navapat Krobkrong, **Vorranutch Itthibenchapong***, Pipat Khongpracha, Deoxygenation of Oleic acid to Produce Bio-hydrogenated Diesel over Molybdenum Oxide Catalysts on Supported Alumina under Inert Atmosphere, NANOTHAILAND 2016, 27-29 November 2016, Nakhon Ratchasima, Thailand. (conference oral presentation abstract)

3.5 Promporn Reangchim, Apiluck Eiad-ua, **Vorranutch Itthibenchapong***, and Kajornsak Faungnawakij, Effect of Sn modification on Ni catalyst for deoxygenation of stearic acid, PACCON 2017, 2-3 February 2017, Bangkok, Thailand. (conference oral presentation abstract)